PERGAMON

International Journal of Heat and Mass Transfer 45 (2002) 2351–2372

International Journal of HEAT and MASS TRANSFER

www.elsevier.com/locate/ijhmt

Development of one-group interfacial area transport equation in bubbly flow systems

Takashi Hibiki [a,*], Mamoru Ishii [b,1]

[a] *Research Reactor Institute, Kyoto University, Kumatori, Sennan, Osaka 590-0494, Japan*
[b] *School of Nuclear Engineering, Purdue University, West Lafayette, IN 47907-1290, USA*

Received 7 January 2001; received in revised form 10 September 2001

Abstract

To finalize one-dimensional one-group interfacial area transport equation in bubbly flow systems, this study has conducted the developments of (I) refined sink and source terms of the interfacial area concentration based on mechanisms of bubble–bubble and bubble–turbulent eddy random collisions, (II) the correlations of two adjustable variables in sink and source terms, and (III) the correlation of the initial interfacial area concentration. The finalized one-dimensional one-group interfacial area transport equation has been validated by 55 data sets taken in extensive adiabatic air–water bubbly flow conditions in four different vertical pipes (pipe diameter: 25.4–50.8 mm). The flow conditions of the data sets cover most of the bubbly flow regime, including finely dispersed bubbly flow and partly bubbly-to-slug transition flow (superficial gas velocity: 0.0144–4.88 m/s, superficial liquid velocity: 0.262–5.00 m/s, void fraction: 0.0124–0.443, interfacial area concentration: 22.1–1085 m^{-1}). Excellent agreement is obtained between predicted and measured interfacial area concentrations with an average relative deviation of ±11.5%. Detailed discussions have been made on (i) the sensitivity analysis to the adjustable variables in the sink and source terms, (ii) the predominant term, (iii) the sensitivity analysis to the initial bubble size, and (iv) the comparison with TRAC-P code.

Keywords: Interfacial area transport; Two-fluid model; Thermal-hydraulics; Thermal-hydraulic code; Gas–liquid bubbly flow; Multiphase flow; Internal pipe flow

1. Introduction

In 1996, the OECD/CSNI Workshop on Transient Thermal-Hydraulic and Neutronic Codes Requirements was held to discuss:

1. current and prospective plans of thermal-hydraulic codes development,
2. current and anticipated uses of thermal-hydraulic codes,
3. advances in modeling of thermal-hydraulic phenomena and associated additional experimental needs,
4. numerical methods in multi-phase flows, and
5. programming language, code architectures and user interfaces [1].

The workshop consensus identified some important action items to be addressed by the international community in order to maintain and improve the calculational capability. One of the important action items is the introduction of the interfacial area transport equation into the interfacial transfer terms in the two-fluid model.

In the present thermal-hydraulic system analysis codes like RELAP5, TRAC and CATHARE, the interfacial area concentration is given by empirical correlations. Ishii and coworkers [2,3] pointed out the following shortcomings caused by the correlations based on traditional two-phase flow regimes and regime transition criteria.

1. The flow regime transition criteria are algebraic relations for steady-state, fully developed flows. They do

* Corresponding author. Tel.: +81-724-51-2373; fax: +81-724-51-2461.

E-mail addresses: hibiki@rri.kyoto-u.ac.jp (T. Hibiki), ishii@ecn.purdue.edu (M. Ishii).

[1] Tel.: +1-765-494-4587; fax: +1-765-494-9570.

0017-9310/02/$ - see front matter
PII: S0017-9310(01)00327-1

Nomenclature

a_i	interfacial area concentration
$\tilde{a}_i$	nondimensional interfacial area concentration
c	parameter defined by D_e/D_b
D	pipe diameter
D_H	equivalent diameter of flow channel
D_b	bubble diameter
$\tilde{D}_b$	nondimensional bubble diameter
$D_{b,max}$	diameter of larger daughter bubble
$D_{b,min}$	diameter of smaller daughter bubble
D_e	eddy diameter
$\overline{E_B}$	energy required for breakup
e	energy of a single eddy
$\overline{e}$	average energy of single eddies
f_B	bubble–eddy random collision frequency
f_C	bubble–bubble random collision frequency
g	gravitational acceleration
j	mixture volumetric flux
j_g	superficial gas velocity
j_f	superficial liquid velocity
K_B	coefficient
K_C	coefficient
k_c	wave number of energy-containing eddies
k_d	wave number of eddies with size of Kolmogoroff microscale
k_e	wave number ($= 2/D_e$)
k_n	wave number of eddies with size of bubble diameter
L	reference length
Lo	Laplace length
$\widetilde{Lo}$	nondimensional Laplace length
m_e	mass per single eddy
N_e	number of eddies of wave number, k_e, per volume of liquid
n_b	bubble number density
n_e	number of eddies with wave number, k_e, per volume of two-phase mixture
$n_{e,max}$	maximum n_e
$n_{e,min}$	minimum n_e
P	pressure
Re	Reynolds number
t	time
t_C	time required for coalescence of bubbles
$\tilde{t}$	nondimensional time
u_b	bubble fluctuating velocity
u_e	eddy velocity
V	characteristic velocity
v_g	time-averaged bubble velocity weighted by void fraction
$\tilde{v}$	nondimensional velocity
We	Weber number
We_{crit}	critical Weber number
z	axial position
$\tilde{z}$	nondimensional axial position

Greeksymbols

α	void fraction
$\alpha_{B,max}$	maximum allowable void fraction
$\alpha_{C,max}$	maximum allowable void fraction
Γ_B	adjustable variable
Γ_C	adjustable variable
γ_B	adjustable variable
γ_C	adjustable variable
δ_{crit}	critical film thickness where rupture occurs
δ_{init}	initial film thickness
$\Delta\rho$	density difference between phases
ε	energy dissipation rate per unit mass
$\tilde{\varepsilon}$	nondimensional energy dissipation rate per unit mass
η	Kolmogoroff microscale
Λ_B	factor defined by Eq. (34)
Λ_C	factor defined by Eq. (33)
Γ_D	factor defined by Eq. (37)
λ_B	bubble breakup efficiency
λ_C	bubble coalescence efficiency
ν_f	kinematic viscosity of liquid
ρ_f	liquid density
ρ_m	mixture density
σ	surface tension
τ_C	contact time for two bubbles
Φ_B	rate of change of interfacial area concentration due to bubble breakup ($= (2a_i/3\alpha)\phi_B$)
Φ_C	rate of change of interfacial area concentration due to bubble coalescence ($= (2a_i/3\alpha)\phi_C$)
Φ_E	rate of change of interfacial area concentration due to bubble expansion ($= (2a_i/3\alpha)\phi_E$)
Φ_P	rate of change of interfacial area concentration due to phase change ($= (2a_i/3\alpha)\phi_P$)
ϕ_B	rate of change of bubble number density due to bubble breakup
ϕ_C	rate of change of bubble number density due to bubble coalescence
ϕ_P	rate of change of bubble number density due to phase change
ψ	factor depending on bubble shape
Ω_B	sensitivity defined by Eq. (32)
Ω_C	sensitivity defined by Eq. (32)

Subscripts

calc.	calculated value
meas.	measured value
0	value at inlet

not fully reflect the true dynamic nature of changes in the interfacial structure. Hence, the effects of the entrance and developing flow can neigther be taken into account correctly nor the gradual transition between regimes.

2. The method based on the flow regime transition criteria is a two-step method, which requires flow configuration transition criteria and interfacial area correlations for each flow configuration. The compound errors from the transition criteria and area correlations can be very significant.
3. The transition criteria and flow-regime-dependent interfacial correlations are valid in limited parameter ranges for certain specific operational conditions and geometries. Most of them are obtained from simple experiments and phenomenological models. Often the scale effects of geometry and fluid properties are not correctly taken into account. When applied to high-to-low-pressure steam–water transients, these models may cause significant discrepancies, artificial discontinuities and numerical instability.

To solve such problems, the introduction of the interfacial area transport equation has been recommended [4–6]. The interfacial area transport equation can be obtained by considering the fluid particle number density transport equation analogous to Boltzmann's transport equation [6]. It can replace the traditional flow regime maps and regime transition criteria. The changes in the two-phase flow structure are predicted mechanistically by introducing the interfacial area transport equation. The effects of the boundary conditions and flow development are efficiently modeled by this transport equation. Such a capability does not exist in the current state-of-the-art codes. Thus, a successful development of the interfacial area transport equation can make a quantum improvement in the two-fluid model formulation [2,3,5,6].

The strategy for the development of the interfacial area transport equation consists of:

1. formulation of the interfacial area transport equation [2,3,6–11],
2. development of measurement techniques [12–21],
3. construction of data base of local flow parameters [19,22–29],
4. modeling of sink and source terms of the interfacial area concentration [7,10,30], and
5. improvement of thermal-hydraulic system analysis codes by implementing the interfacial area transport equation [3,11,31].

In the first stage of the development of the interfacial area transport equation, bubbly flow was the focus, and the one-group interfacial area transport equation was developed by averaging the bubble size over the flow channel [7,30]. The one-group equation has been applied to predicting the interfacial area transport in bubbly flows. Recently, two-group interfacial area transport equations have been proposed by treating the bubbles in two groups, which are the spherical/distorted bubble group and the cap/slug bubble group [2,3,8,10,11]. The two-group equations have been applied to predicting the interfacial area transport at bubbly-to-slug flow transition [10]. The key of successful development of the two-group equations at the bubbly-to-slug flow transition or in the slug and churn flows would certainly be the successful development of the one-group equation in bubbly flow systems.

From this point of view, this study aims at finalizing the one-group interfacial area transport equation in bubbly flow systems and providing detailed discussions on the interfacial area transport in the bubbly flow systems.

2. Development of one-group interfacial area transport equation

2.1. One-group interfacial area transport equation

The interfacial area transport equation can be deduced by considering the fluid particle number density transport equation analogous to Boltzmann's transport equation [6,11]. As a general approach, two-group interfacial area transport equations have recently been proposed by treating the bubbles in two groups such as the spherical/distorted bubble group and the cap/slug bubble group [2,3,8]. This approach results in two interfacial area transport equations that involve the inner and inter group interactions. However, the two-group transport equations can be reduced to one-group for a bubbly flow where the bubbles can be assumed to be equivalent in diameter. With this assumption, the average local particle velocity weighted by the particle number becomes identical to the time-averaged bubble velocity weighted by the gas void fraction, v_g, in the time-averaged two-fluid model [4]. The one-dimensional form of the one-group interfacial area transport equation is given as [7,11,30]

$$\frac{\partial a_i}{\partial t}+\frac{d}{dz}\left(a_i v_g\right)=\frac{1}{3\psi}\left(\frac{\alpha}{a_i}\right)^2\left(\phi_B-\phi_C+\phi_P\right)+\left(\frac{2a_i}{3\alpha}\right)\left\{\frac{\partial\alpha}{\partial t}+\frac{d}{dz}\left(\alpha v_g\right)\right\}=\Phi_B-\Phi_C+\Phi_P+\Phi_E, \tag{1}$$

where

$$\Phi_B\equiv\frac{1}{3\psi}\left(\frac{\alpha}{a_i}\right)^2\phi_B,\quad \Phi_C\equiv\frac{1}{3\psi}\left(\frac{\alpha}{a_i}\right)^2\phi_C,$$

$$\Phi_P\equiv\frac{1}{3\psi}\left(\frac{\alpha}{a_i}\right)^2\phi_P,\quad \Phi_E\equiv\left(\frac{2a_i}{3\alpha}\right)\left\{\frac{\partial\alpha}{\partial t}+\frac{d}{dz}\left(\alpha v_g\right)\right\}.$$

Symbols of a_i, t, z, ψ, α, ϕ_B, ϕ_C, and ϕ_P denote interfacial area concentration, time, axial position, a factor depending on the shape of the bubbles ($\psi = 1/(36\pi)$ for spherical bubbles), void fraction, rate of change of bubble number density due to bubble breakup, rate of change of bubble number density due to bubble coalescence, and rate of change of bubble number density due to phase change, respectively. Φ_B, Φ_C, Φ_P, and Φ_E indicate the rates of change of interfacial area concentration due to bubble breakup, bubble coalescence, phase change, and bubble expansion, respectively.

Under steady-state condition with no phase change, Eq. (1) can be simplified as

$$\frac{d}{dz}(a_i v_g) = \Phi_B - \Phi_C + \Phi_E,$$

$$\text{where } \Phi_E = \left(\frac{2a_i}{3\alpha}\right)\frac{d}{dz}(\alpha v_g). \tag{2}$$

The sink and source terms in the one-group interfacial area transport equation should properly be modeled based on probable mechanisms of bubble coalescence and breakup. Collisions between bubbles may occur due to (a) the turbulent motion of the liquid, (b) differences in individual bubble rise velocities, and (c) the liquid shear [32]. Prince and Blanch [32] found that the main influence on bubble coalescence was the velocity fluctuations of the liquid. On the other hand, the higher the liquid phase turbulence level, the more likely it is that the liquid eddies will break up individual bubbles [33]. In our previous study [30], the main mechanisms of the interfacial area transport have successfully been modeled by the bubble coalescence due to the bubble random collisions driven by turbulence and the bubble breakup due to the impact of turbulent eddies.

It should be noted here that the two-group interfacial area transport equations should be introduced to predict the interfacial area transport at the bubbly-to-slug flow transition or in the slug and churn flows. In these flow regimes, additional bubble coalescence and breakup mechanisms should be taken into account. When large bubbles like cap and slug bubbles are formed, the bubble coalescences between small and large bubbles due to wake entrainment, and between large bubbles due to random collision or wake entrainment would be significant. In addition to these, the breakup of large bubbles due to surface instability and the generation of small bubbles from a skirt of the large bubble due to shearing-off would also be important [7,10]. As will be described later, the developed one-group interfacial area transport equation will be evaluated by using the data set taken in extensive adiabatic air–water bubbly flow conditions. The data sets cover most of the bubbly flow regime, including finely dispersed bubbly flow and partly bubbly-to-slug transition flow. Since the number of cap and slug bubbles is not large at the bubbly-to-slug transition flow ($\alpha \approx 0.25$) in the present data sets, the bubble coalescence due to wake entrainment and the bubble breakup due to shearing-off may not contribute to the interfacial area change significantly [10,29]. Since the bubble size is much smaller than maximum stable bubble size, the bubble breakup due to surface instability is also negligible [10]. Thus, the one-group interfacial area transport equation considering the sink term due to the bubble random collisions and the source term due to the impact of turbulent eddies would approximately be applicable to the bubble-to-slug transition flow in the present data sets where the void fraction is about 0.25. In what follows, the refined models on bubble coalescence and breakup will be described briefly.

2.2. Modeling of bubble coalescence and breakup

The bubble coalescence is considered to occur due to the bubble random collision induced by turbulence in a liquid phase. For the estimation of bubble–bubble collision frequency, f_C, it is assumed that bubbles behave like ideal gas molecules. Furthermore, the following assumptions are made for the modeling of the bubble–bubble collision rate [32]: (i) the turbulence is isotropic; (ii) the bubble size lies in the inertial subrange. Following the kinetic theory of gases [34], the frequency of the collision between a single bubble and surrounding bubbles can be expressed by assuming the identical spherical bubbles as a function of surface available to the collision and volume available to the collision. Taking account of the excluded volume for bubbles and the overlap of the excluded volume for high void fraction region, the final form of the collision frequency is deduced as [30]

$$f_C = \frac{\gamma_C \alpha \varepsilon^{1/3}}{D_b^{2/3}(\alpha_{C,max} - \alpha)}, \tag{3}$$

where γ_C, ε, D_b, and $\alpha_{C,max}$ are an adjustable variable, energy dissipation rate per unit mass, diameter of the bubble, and maximum allowable void fraction, respectively. Since 74.1% of the volume is actually occupied by identical spheres close-packed according to a face-centered cubic lattice [35], $\alpha_{C,max}$ may be assumed to be 0.741.

In order to obtain the bubble coalescence rate, it is necessary to determine a coalescence efficiency, λ_C. The coalescence efficiency is given in terms of the time required for coalescence of bubbles, t_C, and a contact time for the two bubbles, τ_C, as [36]

$$\lambda_C = \exp\left(-\frac{t_C}{\tau_C}\right). \tag{4}$$

The following coalescence efficiency can be derived from the liquid-film-thinning model for t_C [37,38] and the dimensional consideration for τ_C in turbulent flows [39] as

$$\lambda_C = \exp\left(-\frac{K_C \rho_f^{1/2} D_b^{5/6} \varepsilon^{1/3}}{\sigma^{1/2}}\right),$$

$$\text{where } K_C \equiv 2^{-17/6} \ln\frac{\delta_{init}}{\delta_{crit}}, \tag{5}$$

where K_C, ρ_f, σ, δ_{init}, and δ_{crit} are an experimental coefficient to be 1.29 for an air–water system, liquid density, surface tension, initial liquid-film thickness ($= 1\times 10^{-4}$ m for air–water systems) [40], and critical liquid-film thickness ($= 1 \times 10^{-8}$ m for air–water systems) [41], respectively.

The decrease rate of the interfacial area concentration, Φ_C is then expressed as

$$\Phi_C = \frac{1}{3\psi}\left(\frac{\alpha}{a_i}\right)^2 f_C n_b \lambda_C = \frac{\Gamma_C \alpha^2 \varepsilon^{1/3}}{D_b^{5/3}(\alpha_{C,max} - \alpha)} \exp\left(-\frac{K_C \rho_f^{1/2} D_b^{5/6} \varepsilon^{1/3}}{\sigma^{1/2}}\right), \tag{6}$$

where Γ_C and n_b, respectively, are an adjustable variable, and the bubble number density given by

$$n_b = \frac{6\alpha}{\pi D_b^3}. \tag{7}$$

The adjustable variable, Γ_C, would certainly be a function of the overlap of the excluded volume, the bubble deformation, and the bubble velocity distribution. However, in our previous work [30], the adjustable variable was assumed to be a constant for simplicity and was determined experimentally to be 0.0314 for a bubbly flow. The dependence of Γ_C on flow parameters will be discussed later.

On the other hand, the bubble breakup is considered to occur due to the collision of the turbulent eddy with the bubble. For the estimation of bubble–eddy collision frequency, f_B, it is assumed that the eddies and bubbles behave like ideal gas molecules [36]. Furthermore, the following assumptions are made for the modeling of the bubble–eddy collision rate [32]:

1. The turbulence is isotropic.
2. The eddy size, D_e, of interest lies in the inertial subrange.
3. The eddy with the size from $c \cdot D_b$ ($c \leqslant 1$) to D_b can break up the bubble with the size of D_b, since larger eddies have the tendency to transport the bubble rather than to break it and smaller eddies do not have enough energy to break it.

Following the kinetic theory of gases [34], the frequency of the collision between a single turbulent eddy and surrounding bubbles can be expressed by assuming the identical spherical bubbles and spherical eddies as a function of the surface available to the collision and the volume available to the collision. Taking account of the excluded volume for bubbles and eddies, and the overlap of the excluded volume for high void fraction region, the final form of the collision frequency is deduced as [30]

$$f_B = \frac{\gamma_B \alpha \varepsilon^{1/3}}{D_b^{2/3}(\alpha_{B,max} - \alpha)}, \tag{8}$$

where γ_B and $\alpha_{B,max}$ are an adjustable variable depending on c ($\equiv D_e/D_b$) and maximum allowable void fraction, respectively. The maximum allowable void fraction, $\alpha_{B,max}$, in Eq. (8) can approximately be taken at the same value as $\alpha_{C,max}$, namely, 0.741, if eddies with almost the same size of bubbles are assumed to break up the bubbles. Consequently, the functional form of the frequency of the bubble–eddy random collision, Eq. (8) looks similar to that of the frequency of the bubble–bubble random collision, Eq. (3).

In order to obtain the bubble breakup rate, it is necessary to determine a breakup efficiency, λ_B. The breakup efficiency is given in terms of the average energy of a single eddy, $\bar{e}$, and the average energy required for bubble breakup, $\overline{E_B}$, as [32,36,42]

$$\lambda_B = \exp\left(-\frac{\overline{E_B}}{\bar{e}}\right). \tag{9}$$

For binary breakage, that is, the bubble breaks into two bubbles, the required energy, $\overline{E_B}$, is simply calculated as the average value of the energy required for breakage into two equal-size bubbles and a small and a large daughter bubble as follows:

$$\overline{E_B} = \frac{1}{2}\left\{2\pi\sigma\left(\frac{D_b}{2^{1/3}}\right)^2 + \pi\sigma D_{b,max}^2 + \pi\sigma D_{b,min}^2 - 2\pi\sigma D_b^2\right\} = \frac{1}{2}\left\{0.260\pi\sigma D_b^2 + (\pi\sigma D_{b,max}^2 + \pi\sigma D_{b,min}^2 - \pi\sigma D_b^2)\right\}. \tag{10}$$

For the extreme case that $D_{b,max} \to D_b$ and $D_{b,min} \to 0$, $\overline{E_B} = 0.230\pi\sigma D_b^2$. It should be noted here that the relative difference between $\overline{E_B}$ ($= 0.230\pi\sigma D_b^2$) given by Eq. (10) assuming the extreme case and $\overline{E_B}$ ($= 0.260\pi\sigma D_b^2$) assuming the binary breakage into two equal-size bubbles is about 13%. Therefore, the assumption on the size of small and large daughter bubbles may not affect the estimation of $\overline{E_B}$ significantly.

The average energy of single eddies acting on the bubble breakup is simply calculated from

$$\bar{e} = \frac{\int_{n_{e,min}}^{n_{e,max}} e\,dn_e}{\int_{n_{e,min}}^{n_{e,max}} dn_e}, \tag{11}$$

where e and n_e are energy of a single eddy, and number of eddies with wave number, k_e ($= 2/D_e$), per volume of two-phase mixture as given by Eqs. (12) and (14), respectively.

$$e = \frac{1}{2} m_e u_e^2, \tag{12}$$

where m_e and u_e are mass per a single eddy and eddy velocity, respectively. According to Kolmogoroff's law

[43], in the inertial subrange of the energy spectrum, the eddy velocity is given as

$$u_e^2 = 8.2(\varepsilon/k_e)^{2/3}, \tag{13}$$

$$n_e(k_e) = N_e(k_e)(1-\alpha), \tag{14}$$

where $N_e(k_e)$ is number of eddies with wave number, k_e, per volume of fluid as given by [44]

$$\frac{dN_e(k_e)}{dk_e} = 0.1k_e^2. \tag{15}$$

From Eqs. (11)–(15), the average energy of single eddies acting on the bubble breakup is then given by

$$\begin{aligned}\overline{e} &= \frac{\int_{n_{e,min}}^{n_{e,max}} e\,dn_e}{\int_{n_{e,min}}^{n_{e,max}} dn_e} \\ &= \frac{5.46\pi\rho_f\varepsilon^{2/3}0.1(1-\alpha)\int_{k_{e,min}}^{k_{e,max}} k_e^{-5/3}\,dk_e}{0.1(1-\alpha)\int_{k_{e,min}}^{k_{e,max}} k_e^2\,dk_e} \\ &= 1.93\pi\rho_f\varepsilon^{2/3}D_b^{11/3}\frac{1-c^{2/3}}{c^{-3}-1}.\end{aligned} \tag{16}$$

Prince and Blanch [32] set the minimum eddy size, which would not cause bubble breakup, at eddies smaller than 20% of the bubble size, $c^3 = 0.2$. Thus, the average energy of single eddies is expressed by

$$\overline{e} = 0.145\pi\rho_f\varepsilon^{2/3}D_b^{11/3}. \tag{17}$$

The final form of the breakup efficiency is then given by

$$\lambda_B = \exp\left(-\frac{K_B\sigma}{\rho_f D_b^{5/3}\varepsilon^{2/3}}\right), \tag{18}$$

where K_B is a constant to be 1.59 ($= 0.230/0.145$).

The increase rate of the interfacial area concentration, Φ_B is then expressed as

$$\begin{aligned}\Phi_B &= \frac{1}{3\psi}\left(\frac{\alpha}{a_i}\right)^2 f_B n_e \lambda_B \\ &= \frac{\Gamma_B\alpha(1-\alpha)\varepsilon^{1/3}}{D_b^{5/3}(\alpha_{B,max}-\alpha)}\exp\left(-\frac{K_B\sigma}{\rho_f D_b^{5/3}\varepsilon^{2/3}}\right),\end{aligned} \tag{19}$$

where Γ_B is an adjustable variable. The adjustable variable, Γ_B, would certainly be a function of the overlap of the excluded volume, the bubble deformation, the bubble velocity distribution, and the ratio of eddy size to bubble size. However, in our previous work [30], the adjustable variable was assumed to be a constant for simplicity and was determined experimentally to be 0.0209 for a bubbly flow. The dependence of Γ_B on flow parameters will be discussed later.

2.3. Validation of the assumption that the bubble and eddy sizes are in the inertial subrange

In the derivation of sink and source terms, it has been assumed that the bubble and eddy sizes are in the inertial subrange. This assumption is examined here by comparing the wave number of bubbles with the limits of the eddy wave number. The size of the energy-containing eddies is typically assumed to be equal to the length scale of the order of the channel diameter [32]. The experimental conditions of data to be used for the validation of the one-group interfacial area transport equation are shown in Table 1. The channel diameter used in the experiments ranges from 25.4 to 50.8 mm, so

Table 1
Experimental conditions of the existing database used for evaluation of the finalized one-group interfacial area transport equation

Investigators	D (mm), z/D (dimensionless)	Symbols:	○	△	□	▽	◇	*
		j_f (m/s)	$j_{g,0}$ (m/s)	$j_{g,0}$ (m/s)	$j_{g,0}$ (m/s)	$j_{g,0}$ (m/s)	$j_{g,0}$ (m/s)	$j_{g,0}$ (m/s)
Hibiki and Ishii [26]	$D = 25.4$ mm, $z/D = 12, 65, 125$	0.262	0.0549	0.0610	0.0780	0.0990	0.117	N/A
		0.872	0.0414	0.0813	0.143	0.210	0.305	N/A
		1.75	0.0461	0.116	0.257	0.399	0.575	N/A
		2.62	0.0804	0.193	0.401	0.581	0.764	N/A
		3.49	0.0509	0.201	0.516	0.702	0.931	N/A
Hibiki et al. [29]	$D = 50.8$ mm, $z/D = 6, 30, 54$	0.491	0.0275	0.0556	0.129	0.190	N/A	N/A
		0.986	0.0473	0.113	0.242	0.321	N/A	N/A
		2.01	0.103	0.226	0.471	0.624	N/A	N/A
		5.00	0.245	0.518	1.11	1.79	2.87	3.90
Hibiki et al. [19]	$D = 50.8$ mm, $z/D = 2, 32, 62$	0.600	0.0147	0.0205	0.0256	N/A	N/A	N/A
		1.00	0.0186	0.0335	0.0790	N/A	N/A	N/A
		1.30	0.0162	0.0285	0.0763	N/A	N/A	N/A
Grossetete [24]	$D = 38.1$ mm, $z/D = 8, 55, 155$	0.877	0.0588	N/A	N/A	N/A	N/A	N/A
		1.75	0.0577	0.116	N/A	N/A	N/A	N/A

In Grossetete's data, j_g measured at $z/D = 8$ are shown in $j_{g,0}$ columns. N/A: not available.

$k_c \approx 2/D = 0.394$–$0.787\ \mathrm{cm}^{-1}$. On the other hand, the smallest length scale is Kolmogoroff microscale, η, given by [45]

$$\eta = \left(\frac{v_f^3}{\varepsilon}\right)^{1/4}, \tag{20}$$

where v_f is kinematic viscosity of the liquid. The wave number, k_d, where the viscous effects become very strong will be of the same order as $1/\eta$. It is usual to define k_d in such a way that $k_d = 1/\eta$ [45]. The microscale η ranges from 10^{-4} to 10^{-3} cm over the experimental range shown in Table 1, so $k_d = 10^3$ to $10^4\ \mathrm{cm}^{-1}$. The average bubble size at this energy dissipation ranges from 1 to 5 mm in diameter, so $k_n = 4$ to $20\ \mathrm{cm}^{-1}$. Thus, $k_c \ll k_n \ll k_d$, which indicates that the length scales of the bubble and the eddy acting on the bubble breakup are in the inertial subrange. This situation will similarly apply in most industrial scale pipe flows.

2.4. Nondimensionalization of one-group interfacial area transport equation

The one-group interfacial area transport equation with no phase change is nondimensionalized here to discuss the flow-parameter dependence of this equation. From Eqs. (1), (6) and (19), the one-dimensional form of the one-group interfacial area transport equation with no phase change is given as

$$\begin{aligned}\frac{\partial a_i}{\partial t} + \frac{\mathrm{d}}{\mathrm{d}z}(a_i v_g) &= -\frac{\Gamma_C \alpha^2 \varepsilon^{1/3}}{D_b^{5/3}(\alpha_{C,\max} - \alpha)} \exp\left(-\frac{K_C \rho_f^{1/2} D_b^{5/6} \varepsilon^{1/3}}{\sigma^{1/2}}\right) \\ &\quad + \frac{\Gamma_B \alpha (1-\alpha) \varepsilon^{1/3}}{D_b^{5/3}(\alpha_{B,\max} - \alpha)} \exp\left(-\frac{K_B \sigma}{\rho_f D_b^{5/3} \varepsilon^{2/3}}\right) \\ &\quad + \frac{4}{D_b}\left\{\frac{\partial \alpha}{\partial t} + \frac{\mathrm{d}}{\mathrm{d}z}(\alpha v_g)\right\}.\end{aligned} \tag{21}$$

Here, the bubble size, D_b, is given as

$$D_b = \frac{6\alpha}{a_i}. \tag{22}$$

The interfacial area transport equation can be nondimensionalized as follows: Let

$$\begin{aligned}&\tilde{v} \equiv \frac{v_g}{V}, \quad \tilde{z} \equiv \frac{z}{L}, \quad \tilde{D}_b \equiv \frac{D_b}{L}, \quad \tilde{t} \equiv \frac{tV}{L}, \\ &\tilde{\varepsilon} \equiv \frac{\varepsilon L}{V^3}, \quad \tilde{a}_i \equiv a_i L,\end{aligned} \tag{23}$$

where V and L are a characteristic velocity and a reference length, respectively. As will be discussed later, v_f/Lo and Lo can be taken as the characteristic velocity and the reference length, respectively. Here, Lo is the Laplace length (or capillary length) defined by

$$Lo \equiv \sqrt{\frac{\sigma}{g\Delta\rho}}. \tag{24}$$

The Laplace length characterizes the bubble diameter length scale. The nondimensionalized one-dimensional form of the one-group interfacial area transport equation can then be written as

$$\begin{aligned}\frac{\partial \tilde{a}_i}{\partial \tilde{t}} + \frac{\mathrm{d}}{\mathrm{d}\tilde{z}}(\tilde{a}_i \tilde{v}_g) &= -\frac{\Gamma_C \alpha^2 \tilde{\varepsilon}^{1/3}}{\tilde{D}_b^{5/3}(\alpha_{C,\max} - \alpha)} \exp(-K_C\sqrt{We}) \\ &\quad + \frac{\Gamma_C \alpha (1-\alpha) \tilde{\varepsilon}^{1/3}}{\tilde{D}_b^{5/3}(\alpha_{B,\max} - \alpha)} \exp(-K_B/We) \\ &\quad + \frac{4}{\tilde{D}_b}\left\{\frac{\partial \alpha}{\partial \tilde{t}} + \frac{\mathrm{d}}{\mathrm{d}\tilde{z}}(\alpha \tilde{v}_g)\right\},\end{aligned} \tag{25}$$

where We is the Weber number defined by

$$We \equiv \frac{\rho_f (\varepsilon^{1/3} D_b^{1/3})^2 D_b}{\sigma} = \frac{\rho_f \varepsilon^{2/3} D_b^{5/3}}{\sigma}. \tag{26}$$

It should be noted here that the bubble velocity in the inertial subrange of isotropic turbulence, u_b, can be represented as $u_b \propto \varepsilon^{1/3} D_b^{1/3}$ [46]. Under steady-state condition with no phase change, Eq. (25) can be simplified as

$$\begin{aligned}\frac{\mathrm{d}}{\mathrm{d}\tilde{z}}(\tilde{a}_i \tilde{v}_g) &= -\frac{\Gamma_C \alpha^2 \tilde{\varepsilon}^{1/3}}{\tilde{D}_b^{5/3}(\alpha_{C,\max} - \alpha)} \exp(-K_C\sqrt{We}) \\ &\quad + \frac{\Gamma_C \alpha (1-\alpha) \tilde{\varepsilon}^{1/3}}{\tilde{D}_b^{5/3}(\alpha_{B,\max} - \alpha)} \exp(-K_B/We) \\ &\quad + \frac{4}{\tilde{D}_b}\frac{\mathrm{d}}{\mathrm{d}\tilde{z}}(\alpha \tilde{v}_g).\end{aligned} \tag{27}$$

3. Results and discussions

3.1. Databases used for evaluation of one-group interfacial area transport equation and calculation procedure

To evaluate the one-dimensional one-group interfacial area transport equation, the present authors measured axial developments of void fraction, interfacial area concentration, gas and liquid velocities and pressure for adiabatic air–water bubbly flows in vertical pipes at the Thermal-hydraulics and Reactor Safety Laboratory in Purdue University [19,26,29]. The radial profiles of gas and liquid phases were obtained by the double sensor probe and hotfilm anemometry at three axial locations. One-dimensional flow parameters were

calculated by integrating the radial profiles over the flow channel. The measurement accuracies of the one-dimensional flow parameters were confirmed by other cross-calibration methods such as γ-densitometer, photography, rotameter and magnetic flow meter for void fraction, interfacial area concentration, gas velocity and liquid velocity, respectively. The average relative deviations for measurements of void fraction, interfacial area concentration, gas velocity and liquid velocity between the probe methods and the cross-calibration methods were ±5.74%, ±6.95%, ±12.4% and ±5.19%, respectively [26,29]. In addition to our databases, the data taken by Grossetete [24] is also available. Table 1 shows the experimental conditions of the databases to be used for evaluation of the interfacial area transport equation.

To evaluate the one-group interfacial area transport equation, axial development of void fraction, gas velocity and energy dissipation rate per unit mass, and interfacial area concentration at the inlet should be given as accurately as possible. The void fraction and gas velocity are given by empirical correlations [30] based on the measured values. The energy dissipation rate per unit mass is simply calculated from the mechanical energy equation [30,47] as

$$\varepsilon = \frac{j}{\rho_m}\left(-\frac{dP}{dz}\right)_F, \tag{28}$$

where j, ρ_m, and $(-dP/dz)_F$ are the mixture volumetric flux, the mixture density, and the gradient of the frictional pressure loss along the flow direction, respectively. The two-phase frictional pressure loss is estimated by Lockhart–Martinelli's method [48]. The estimation uncertainty of the energy dissipation rate per unit mass is easily adjusted by the adjustable variables, Γ_C and Γ_B. The initial values of the interfacial area concentrations are given by those measured at the first measuring station or an empirical correlation described later as Eq. (31). The average effect of the bubble deformation on the interfacial area concentration is also adjusted by the adjustable variable, Γ_C and Γ_B to be determined experimentally. The interfacial area concentration in the flow direction is calculated by a finite difference method. The propagated error caused by the uncertainty of these component models is estimated to be ±12.2% with the measured interfacial area concentration at the first measuring station, or ±15.7% with the empirical correlation as the initial value of the interfacial area concentration.

3.2. Development of correlations of adjustable variables, Γ_C and Γ_B

As pointed out in the previous section, the adjustable variables, Γ_C and Γ_B, would be a function of the overlap of the excluded volume, the bubble deformation, and the bubble velocity distribution. The overlap of the excluded volume would certainly be a function of the void fraction. The bubble deformation may be characterized by the Weber number. Since the bubble velocity in the inertial subrange of isotropic turbulence, u_b, can be represented as $u_b \propto \varepsilon^{1/3} D_b^{1/3} \approx \varepsilon^{1/3} Lo^{1/3}$ [46], the bubble velocity distribution is expected to be characterized by the energy dissipation rate per unit mass and Laplace length. It is difficult to develop universal correlation of the adjustable variables because of limited database so far. Here, the adjustable variables are simply assumed to be given by the product of the void fraction and the nondimensionalized energy dissipation rate per unit mass, $\tilde{\varepsilon}$ defined by $\tilde{\varepsilon} \equiv Lo^4(\varepsilon/v_f^3)$. The coefficients of the functions are then determined from 55 data sets on the interfacial area transport listed in Table 1. Finally,

$$\Gamma_C = 1.82 \times 10^{-8} \alpha \tilde{\varepsilon} = 1.82 \times 10^{-8}\, \alpha Re^3$$

and

$$\Gamma_B = 5.02 \times 10^{-10} \alpha \tilde{\varepsilon} = 5.02 \times 10^{-10}\, \alpha Re^3, \tag{29}$$

where Re is the Reynolds number defined by

$$Re \equiv \frac{(\varepsilon^{1/3} Lo^{1/3}) Lo}{v_f} = \tilde{\varepsilon}^{1/3}.$$

Fig. 1 shows examples of the comparison of calculated results with the existing data sets. In figures, solid and dotted lines indicate the calculated interfacial area concentrations using Eq. (29), and the constant coefficients of $\Gamma_C = 0.0314$ and $\Gamma_B = 0.0209$ determined in our previous study [30], respectively. In the interfacial area transport calculation, the interfacial area concentrations measured at the first measuring station are used as the initial values. The meanings of symbols in these figures are explained in Table 1. As shown in Fig. 1, newly developed correlations of the adjustable variables, Γ_C and Γ_B can reproduce better trends of the interfacial area transport in the flow direction than the constant adjustable variables. Similar results are obtained for the other experimental conditions shown in Table 1. The introduction of the new correlations of the adjustable variables into the one-group interfacial area transport equation improves the prediction accuracy significantly. Eq. (29) appears to characterize the dependence of the adjustable variables, Γ_C and Γ_B on the overlap of the excluded volume, the bubble deformation, and the bubble velocity distribution appropriately. However, further study such as the development of extensive database should be indispensable to develop the universal correlation of the adjustable variables.

3.3. Development of correlation of initial interfacial area concentration

To finalize the one-group interfacial area transport equation, the correlation of the initial interfacial area

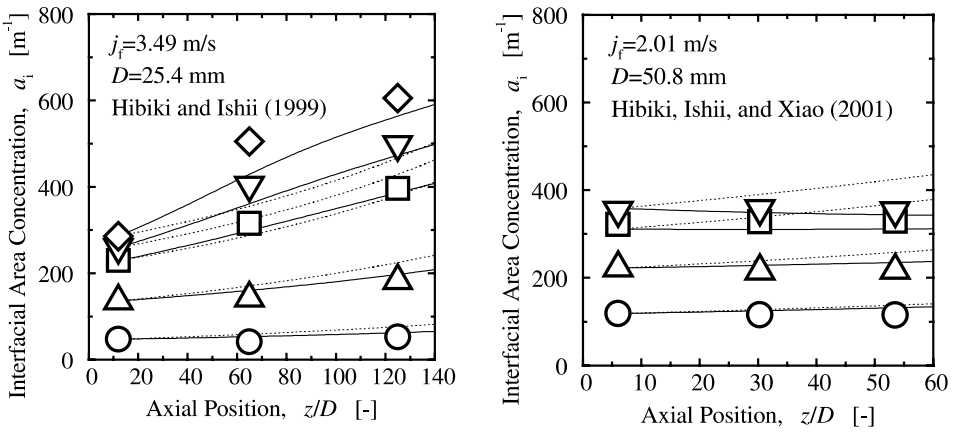

Fig. 1. Comparison between predictions by one-group interfacial area transport equation using correlation of adjustable variables, Eq. (29) in sink and source terms (solid lines) and those using constant adjustable variables, $\Gamma_C = 0.0314$ and $\Gamma_B = 0.0209$ (dotted lines).

concentration should be developed. In our previous study [49], a correlation of the interfacial area concentration under steady fully developed bubbly flow conditions was successfully developed by deducing the flow-parameter dependence of the interfacial area correlation from the interfacial area transport equation. It was shown analytically that the parameters governing the interfacial area concentration of steady fully developed bubbly flows should be (σ/ρ_f), α, and ε [49]. In the end, the correlation of the interfacial area concentration under steady fully developed bubbly flow conditions has been proposed based on experimental data and detailed length-scale analysis as

$$\tilde{a}_i = 0.500\widetilde{Lo}^{-0.283}\alpha^{0.847}\tilde{\varepsilon}^{0.0707} = 0.500\widetilde{Lo}^{-0.283}\alpha^{0.847}Re^{0.212}, \quad (30)$$

where

$$\tilde{a}_i \equiv \frac{a_i}{Lo^{-1}} \quad \text{and} \quad \widetilde{Lo} \equiv Lo/D_H.$$

Here, D_H is equivalent diameter of the flow channel. Eq. (30) has been validated by 204 data sets measured in steady fully developed air–water bubbly flows [49]. The data sets used in the validation covered extensive flow and loop conditions including as channel geometry (circular or rectangular channel), flow direction (vertical or horizontal flow), superficial gas velocity (0.018–4.87 m/s), superficial liquid velocity (0.262–6.55 m/s) and interfacial area concentration (25.8–1083 m^{-1}). An excellent agreement was obtained between the developed semi-theoretical correlation, Eq. (30), and the data with an average relative deviation of ±11.1%. The interfacial area concentration representing the interfacial structure length scale is characterized by the internal length scale such as the Laplace length, the system length scale such as the hydraulic equivalent diameter of the flow channel, the space probability such as the void fraction, the parameter governing the bubble coalescence and breakup, and the flow field such as the Reynolds number.

To develop a correlation, the interfacial area concentration at the inlet, $a_{i,0}$, is assumed to have the same flow-parameter dependence as a_i. Since the data of the interfacial area concentration just at the inlet are not available, the data of the interfacial area concentration measured at the first measuring station are used to develop the correlation at the inlet. In a strict sense, the correlation to be developed is for the interfacial area concentration at the first measuring station. The correlation of the initial interfacial area concentration is then obtained based on 55 data sets measured at the first measuring station as

$$\tilde{a}_{i,0} = 1.64\widetilde{Lo}_0^{-0.127}\alpha_0^{0.851}\tilde{\varepsilon}_0^{0.0318}, \quad (31)$$

where $\tilde{a}_{i,0}$, $\widetilde{Lo}_0$, α_0, and $\tilde{\varepsilon}_0$ are the initial values of the nondimensional interfacial area concentration, the nondimensional Laplace length, the void fraction, and the nondimensional energy dissipation rate per unit mass, respectively. As shown in Fig. 2, the above correlations can predict the interfacial area concentration at the first measuring station with an average relative deviation of ±12.1%. The interfacial area concentration just at the inlet can be evaluated by extrapolating Eq. (31) to the inlet.

It is known that the initial bubble size, namely the initial interfacial area concentration is affected by the bubble distributor design. Thus, in a strictly sense, the applicability of Eq. (31) should be limited to the tested experimental conditions. However, on the following grounds, Eq. (31) may presumably be applicable to experimental conditions over the tested ones except for extreme flow conditions such as extremely low liquid flow and injection of slug bubbles. Millies and Mewes

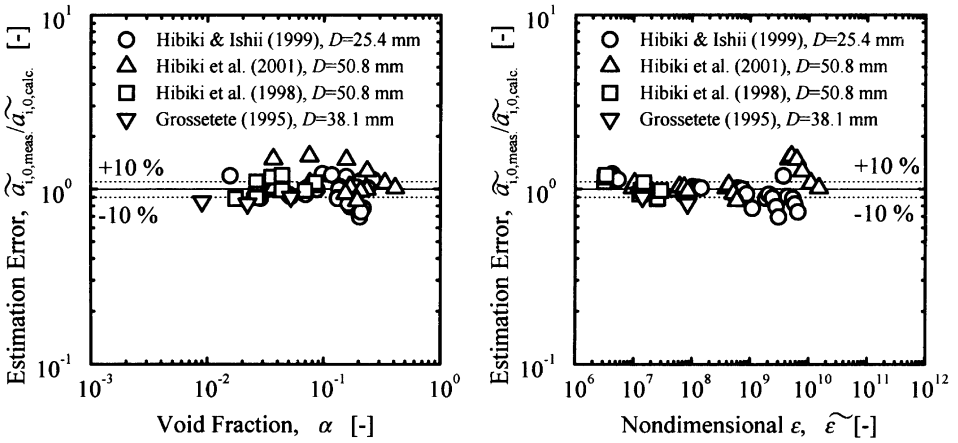

Fig. 2. Comparison of developed initial interfacial area correlation, Eq. (31), with existing data.

classified the bubble coalescence and breakup process in a bubble column into four basic processes in the flow direction such as (a) primary bubbles, (b) secondary bubbles, (c) bubble coalescence and breakup come to an equilibrium state, and (d) coalescence with the free surface, eventually formation of foam [50]. The size of primary bubbles is strongly influenced by the bubble distributor design. The primary bubbles would coalesce and breakup violently in the vicinity of the bubble distributor, and reach to the secondary bubbles. The size of the secondary bubbles would be a weak function of the bubble distributor design. This is particularly true for high liquid velocity condition. The axial length for primary bubble region may be a function of liquid velocity and initial bubble size distribution. Judging from the present test data, the bubble coalescence and breakup process seem to reach the secondary bubble region even at the first measuring station, since the interfacial area transport at the downstream of the first measuring station is quite smooth and is well characterized by the one-group interfacial area transport equation considering the bubble coalescence and breakup. As Eq. (31) was developed based on the data sets taken at the first measuring station, it would be promising for the evaluation of the initial bubble size except for extreme flow conditions such as extremely low liquid flow and injection of slug bubbles.

3.4. Comparison of finalized one-group interfacial area transport equation with experimental data

The one-dimensional one-group interfacial area transport equation has been finalized by introducing newly developed correlations of the adjustable variables, Eq. (29), and the initial interfacial area concentration, Eq. (31). Figs. 3–6 show the comparisons of the finalized one-dimensional one-group interfacial area transport equation with the existing 55 data sets measured in four different flow loops (25.4 mm $\leqslant D \leqslant$ 50.8 mm). These data sets cover extensive flow conditions such as superficial gas velocity from 0.0144 to 4.88 m/s, superficial liquid velocity from 0.262 to 5.00 m/s, void fraction from 0.0124 to 0.443, and interfacial area concentration from 22.1 to 1085 m^{-1}. The corresponding flow regimes include bubbly flow, finely dispersed bubbly flow, and partly bubbly-to-slug transition flow. The meanings of symbols in these figures are explained in Table 1. It can be recognized that the finalized one-group interfacial area transport equation can reproduce proper trends of the interfacial area transport depending on flow parameters. As a general trend, the pressure term, Φ_E, governs the interfacial area transport at relatively low liquid velocity and void fraction, where bubble–bubble and bubble–eddy interactions are weak. The bubble coalescence term, Φ_C, is enhanced in the interfacial area transport equation at high void fraction, where the bubble distance is short enough to cause the bubble coalescence. On the other hand, the bubble breakup terms, Φ_B, plays an important role in the interfacial area transport equation at relatively high liquid velocity, where the liquid turbulence is strong enough to disintegrate bubbles. The detailed discussions on the predominant terms will be given later. As shown in Fig. 7, the finalized one-dimensional one-group interfacial area transport equation with only two adjustable variables gives excellent predictions of the interfacial area concentrations ranging over two orders with an average deviation of ±11.5%.

3.5. Sensitivity analysis on adjustable variables in sink and source terms in the interfacial area transport equation

Here, the sensitivity analysis on the adjustable variables, Γ_C and Γ_B, in sink and source terms is performed

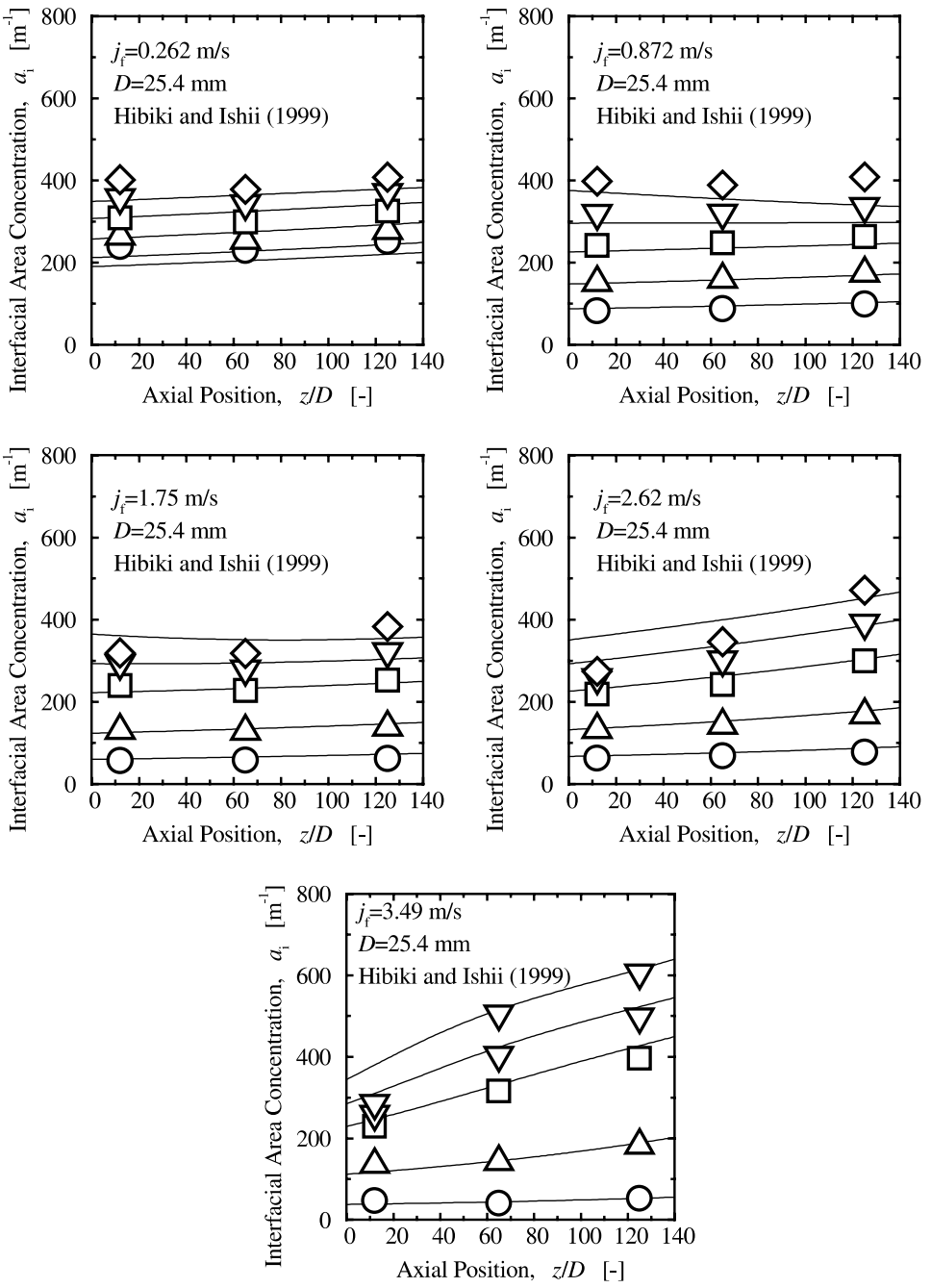

Fig. 3. Comparison of measured interfacial area concentrations of vertical bubbly flows in a 25.4 mm-diameter pipe [26] with predictions by finalized one-group interfacial area transport equation.

to investigate the dependence of the predicted value of the interfacial area concentration on the adjustable variables. The sensitivities, Ω_C and Ω_B are defined by

$$\Omega_C \equiv \frac{a_i(\Lambda_C)}{a_i(\Lambda_C = 1)} \quad \text{and} \quad \Omega_B \equiv \frac{a_i(\Lambda_B)}{a_i(\Lambda_B = 1)}, \tag{32}$$

where Λ_C and Λ_B are the factors defined by the ratio of the adjustable variables used in the sensitivity analysis to those calculated by Eq. (29) as defined by Eqs. (33) and (34), respectively.

$$\Lambda_C = \frac{\Gamma_C}{1.82 \times 10^{-8} \alpha \tilde{\varepsilon}}, \tag{33}$$

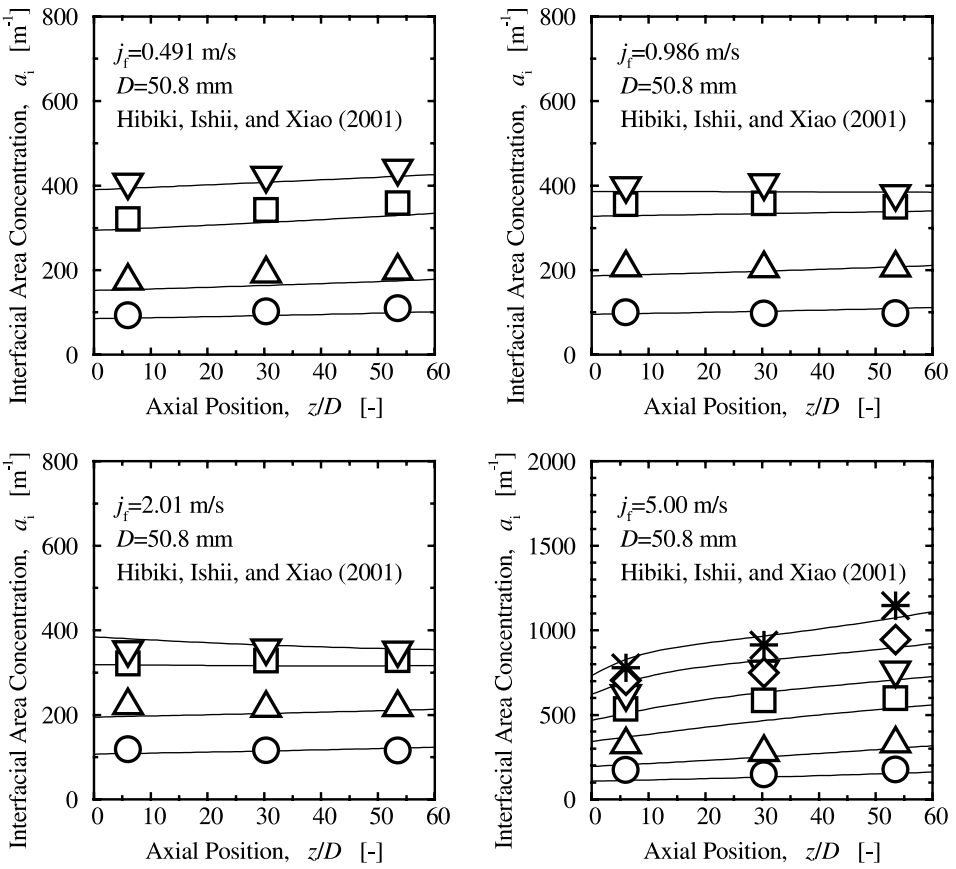

Fig. 4. Comparison of measured interfacial area concentrations of vertical bubbly flows in a 50.8 mm-diameter pipe [29] with predictions by finalized one-group interfacial area transport equation.

$$\Lambda_B = \frac{\Gamma_B}{5.02 \times 10^{-10} \alpha \tilde{\varepsilon}}, \tag{34}$$

where $a_i(\Lambda_C)$ and $a_i(\Lambda_B)$ are the interfacial area concentrations calculated by the one-group interfacial area transport equation with the adjustable variables of $\Gamma_C = \Lambda_C \times 1.82 \times 10^{-8} \alpha \tilde{\varepsilon}$ and $\Gamma_B = 5.02 \times 10^{-10} \alpha \tilde{\varepsilon}$, and of $\Gamma_C = 1.82 \times 10^{-8} \alpha \tilde{\varepsilon}$ and $\Gamma_B = \Lambda_B \times 5.02 \times 10^{-10} \alpha \tilde{\varepsilon}$, respectively. The sensitivity analysis is performed by using flow parameters measured in a 50.8 mm-diameter pipe at $z/D = 54$ [29]. Figs. 8 and 9 show the results of the sensitivity analyses for Γ_C and Γ_B, respectively. As expected by Eq. (6), the interfacial area concentration is not so sensitive to the change of Γ_C at low void fraction. The sensitivity, Ω_C, is affected more at higher void fraction and superficial liquid velocity. On one hand, the interfacial area concentration is not sensitive to the change of Γ_B at low superficial liquid velocities such as $j_f = 0.491$ and 0.986 m/s. As will be discussed later, for such low liquid velocities, the breakup efficiency is negligibly low, resulting in no sensitivity of Γ_B to the interfacial area concentration. As expected by Eq. (19), the sensitivity, Ω_B, is affected more at higher void fraction and superficial liquid velocity.

3.6. Predominant term analysis

Fig. 10 shows results from the scale analysis to identify the predominant term among the sink and source terms for the data taken in a 50.8 mm-diameter pipe [29]. The figure at upper left shows the contribution of the bubble coalescence to the interfacial area transport, which is normalized by the bubble expansion term, namely Φ_C/Φ_E. In the case of low void fraction and superficial liquid velocity, the contribution of the bubble coalescence can be neglected compared with the contribution of the bubble expansion by the pressure reduction. As the void fraction and superficial liquid velocity increase, the contribution of bubble coalescence comes to be comparable to or larger than that of the pressure reduction.

The figure at upper right shows the contribution of the bubble breakup, which is normalized by the bubble expansion term, namely Φ_B/Φ_E. Under the low liquid flow conditions such as $j_f = 0.491$ and 0.986 m/s, the

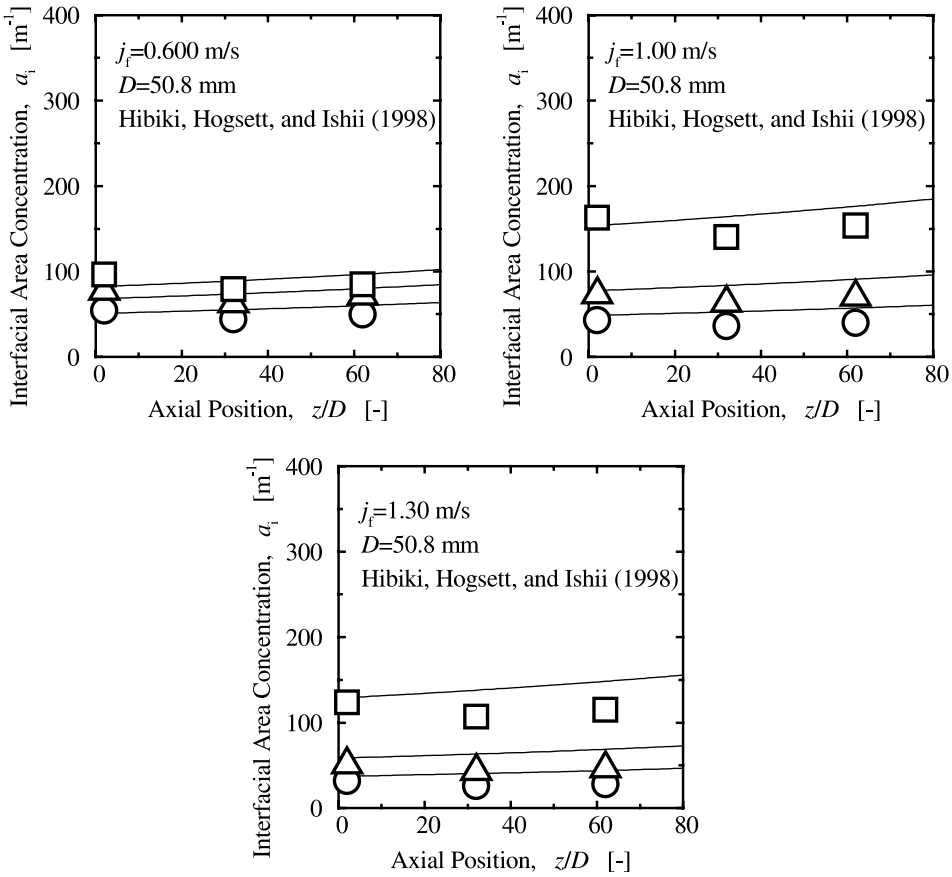

Fig. 5. Comparison of measured interfacial area concentrations of vertical bubbly flows in a 50.8 mm-diameter pipe [19] with predictions by finalized one-group interfacial area transport equation.

contribution of the bubble breakup is negligibly small because of negligibly low breakup efficiency (see the figure at the lower right). On the other hand, under the high liquid flow conditions such as $j_f = 2.01$ and 5.00 m/s, the contribution of the bubble breakup comes to be marked.

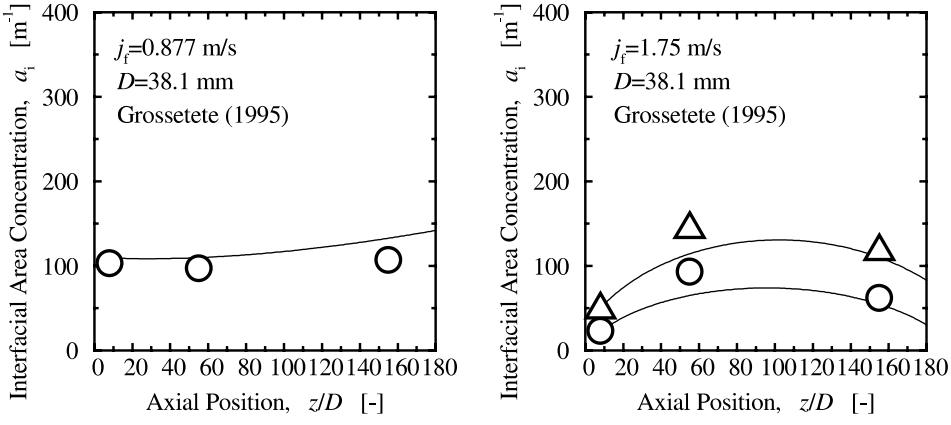

Fig. 6. Comparison of measured interfacial area concentrations of vertical bubbly flows in a 38.1 mm-diameter pipe [24] with predictions by finalized one-group interfacial area transport equation.

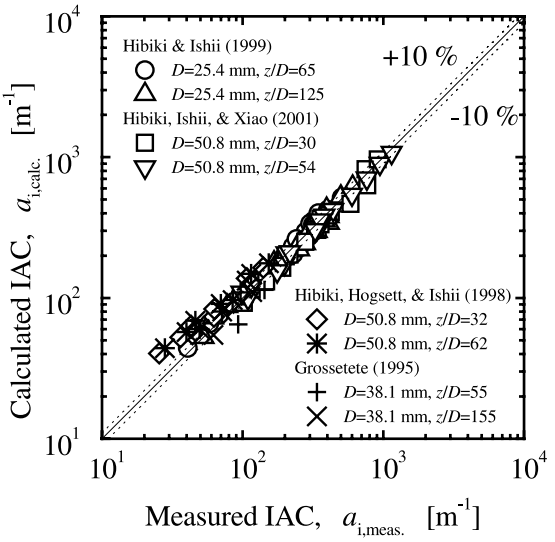

Fig. 7. Comparison of measured interfacial area concentrations with predictions by finalized one-group interfacial area transport equation.

Figure at lower left of Fig. 10 shows the predominant mechanism of the interfacial area transport. At low superficial liquid velocities such as $j_f = 0.491$, 0.986, and 2.01 m/s, bubble coalescence is dominant over bubble breakup because of small turbulence, whereas bubble breakup becomes dominant over bubble coalescence at high superficial liquid velocity of $j_f = 5.00$ m/s. In the finely dispersed bubbly flow region with void fraction higher than 30%, the contribution of bubble breakup comes to be comparable to bubble coalescence.

Fig. 11 shows the dependence of the bubble diameter measured at $z/D = 54$ on the void fraction and superficial liquid velocity. Since the initial bubble sizes are not controlled in the experiment, the experimental result suggests rough flow-parameter dependence of the bubble diameter. Based on Eq. (7), the bubble size changes in proportion to the 1/3 power of the void fraction and the $-1/3$ power of the bubble number density. This means that the bubble breakup mitigates the increase in the bubble diameter arising from the void fraction increase. As shown in the left figure of Fig. 11, lower increase rate

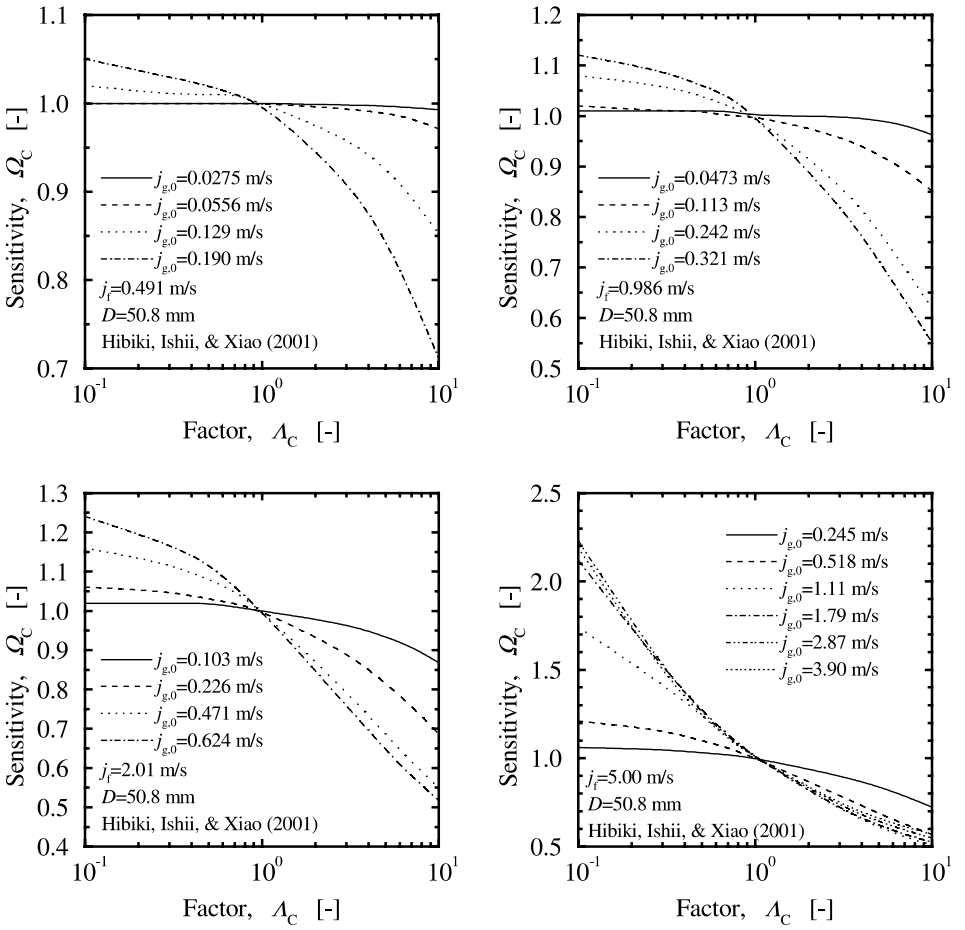

Fig. 8. Sensitivity analysis on adjustable variable, Γ_C, in sink term.

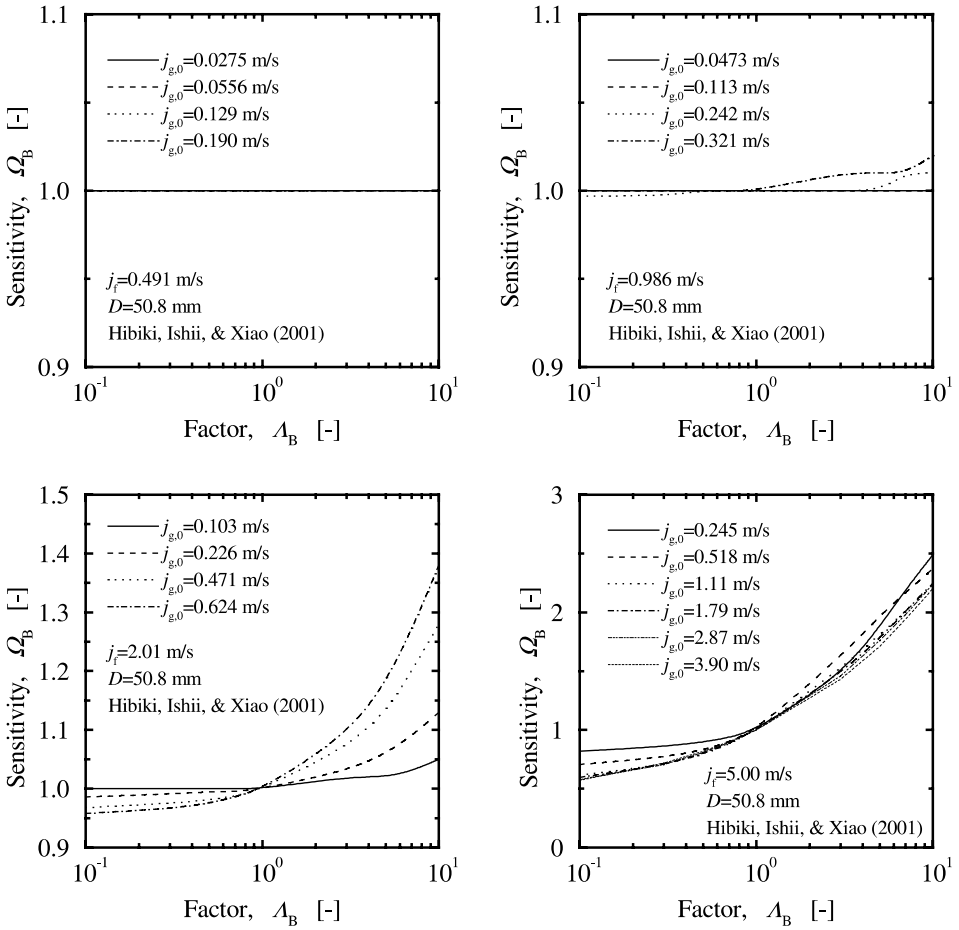

Fig. 9. Sensitivity analysis on adjustable variable, Γ_B, in source term.

of the bubble diameter to void fraction for $j_f = 5.00$ m/s in comparison with those for $j_f = 0.491$, 0.986, and 2.01 m/s suggests that significant bubble breakup may occur for $j_f = 5.00$ m/s.

As shown in the right figure of Fig. 11, the bubble diameter increases with the superficial liquid velocity where $j_f \leqslant 1$ m/s, whereas it markedly decreases where $j_f \geqslant 2$ m/s. The enhanced turbulence due to the increased superficial liquid velocity appears to contribute mainly to the bubble coalescence or the bubble breakup for $j_f \leqslant 1$ m/s or for $j_f \geqslant 2$ m/s, respectively. The fact that the contribution of the bubble breakup is steeply increased around $j_f = 2$ to 5 m/s can be related with a critical Weber number. The criterion for breakup relates the energy of the eddy to the surface tension forces of the bubble. The balance of disruptive and cohesive forces is generally expressed in terms of the Weber number. The critical Weber number will exist at the point where cohesive and disruptive forces balance, resulting in a maximum stable bubble size [32]. In a forced convective pipe flow or mechanically agitated systems, the initial bubble size may be too large or too small to be stable. In these cases, the bubble size is further determined by a breakup and/or coalescence mechanism [6]. As known well, finely dispersed bubbly flow is observed for high superficial liquid velocity. Taitel et al. [51] modeled the criteria of flow regime transition between bubbly flow and finely dispersed bubbly flow as follows. For high superficial liquid flow, bubble breakup would occur due to turbulent forces so that coalescence would also be prevented above a limit on the sum of j_f and j_g derived as

$$j_g + j_f = 4\left[\frac{D^{0.429}(\sigma/\rho_f)^{0.089}}{\nu_f^{0.072}}\left\{\frac{g\Delta\rho}{\rho_f}\right\}^{0.446}\right]. \quad (35)$$

The superficial liquid velocity at the flow regime transition boundary is estimated to be about 3.5 m/s for $D = 50.8$ mm, corresponding to the superficial liquid velocity where the contribution of breakup to interfacial area transport is steeply enhanced. Here, a critical Weber number, We_{crit}, is defined as the Weber number at the equilibrium state of the bubble coalescence and breakup.

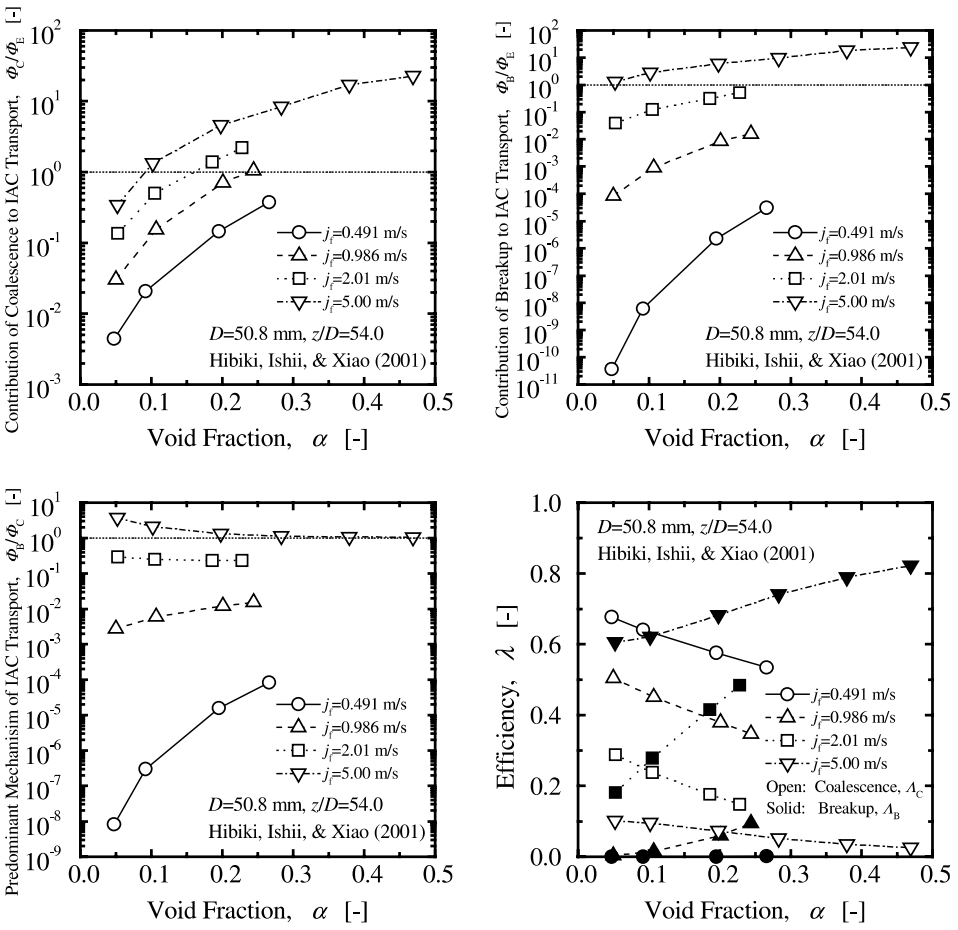

Fig. 10. Predominant term analysis.

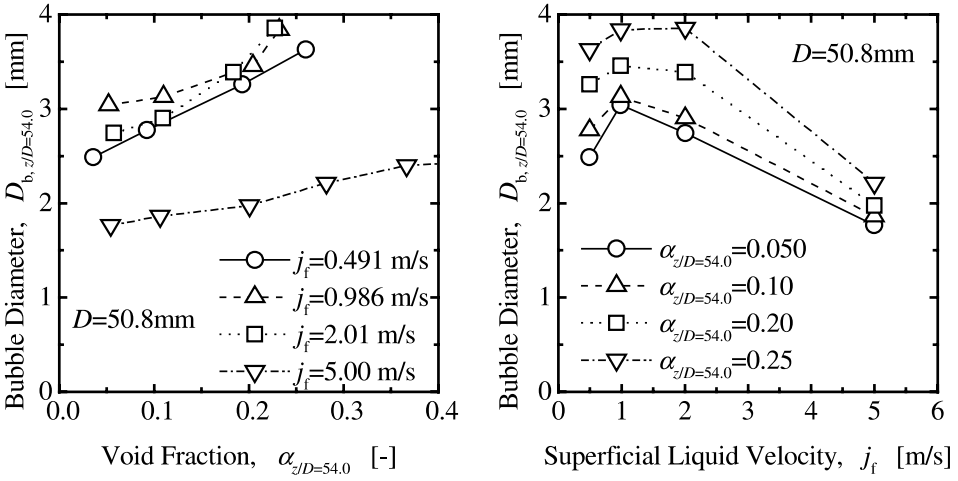

Fig. 11. Dependence of bubble diameter on void fraction and superficial liquid velocity.

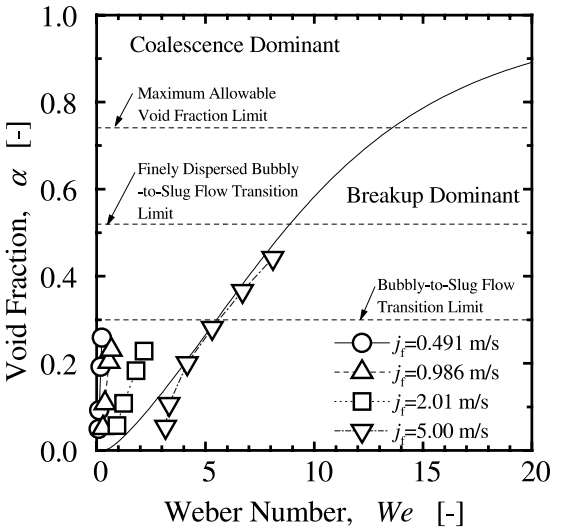

Fig. 12. Dependence of dominant phenomena for interfacial area concentration change on critical Weber number.

The relationship between the void fraction and the critical Weber number can be derived from Eq. (27) by equating the sink term with the source term as

$$\alpha = \frac{(\Gamma_B/\Gamma_C)\exp(-K_B/We_{crit} + K_C\sqrt{We_{crit}})}{1 + (\Gamma_B/\Gamma_C)\exp(-K_B/We_{crit} + K_C\sqrt{We_{crit}})}. \quad (36)$$

Fig. 12 shows the relationship between the void fraction and the Weber number. Open symbols and a solid line indicate the values calculated by Eq. (26) with experimental data measured at $z/D = 54$ and the critical Weber number calculated by Eq. (36), respectively. The data for $j_f = 0.491$, 0.986, and 2.01 m/s exist in the bubble coalescence dominant region, whereas the data for $j_f = 5.00$ m/s exist in the bubble breakup dominant region even for $\alpha \geqslant 0.3$. This bubble breakup dominant flow condition sustains the bubbly flow even for $\alpha \geqslant 0.3$, which corresponds to the finely dispersed bubbly flow. Thus, the interfacial area transport equation can also explain the flow regime transition between bubbly flow and finely bubbly flow qualitatively.

3.7. Sensitivity analysis to initial bubble size

The sensitivity analysis of the interfacial area concentration to the initial bubble size is performed here to investigate the effect of the initial bubble size on the interfacial area transport. Here, the factor, Λ_D, is defined as

$$\Lambda_D = \frac{D_{b,0}}{D_{b,0,calc.}}, \quad (37)$$

where $D_{b,0,calc.}$ is the bubble diameter calculated by Eqs. (22) and (31).

Fig. 13 depicts the sensitivity analyses for bubbly flows in a 50.8 mm-diameter pipe. The flow conditions are (a) $j_f = 0.491$ m/s and $j_{g,0} = 0.190$ m/s ($\alpha_{z/D=53.5} = 0.259$), (b) $j_f = 0.986$ m/s and $j_{g,0} = 0.321$ m/s ($\alpha_{z/D=53.5} = 0.231$), (c) $j_f = 2.01$ m/s and $j_{g,0} = 0.624$ m/s ($\alpha_{z/D=53.5} = 0.228$), and (d) $j_f = 5.00$ m/s and $j_{g,0} = 3.90$ m/s ($\alpha_{z/D=53.5} = 0.442$). For the low superficial liquid velocities such as $j_f = 0.491$ and 0.986 m/s, the interfacial area transport calculation suggests that the effect of the initial bubble size on the interfacial area concentration remains even at the axial position far from the inlet. This is attributed to insignificant bubble coalescence and breakup because of small turbulence fluctuation. Interestingly, as the superficial liquid velocity increases, the effect of the initial bubble size on the interfacial area concentration comes to disappear at a certain distance from the inlet because of significant bubble interaction. For $j_f = 5.00$ m/s, the effect of the initial bubble size completely disappears at $z/D = 30$. For large initial bubble size, significant bubble breakup increases the interfacial area concentration, whereas for small initial bubble size, significant bubble coalescence decreases the interfacial area concentration. Thus, the dominant mechanism of the bubble interaction appears to be dependent on the initial bubble size. It is expected that for high liquid velocity the one-group interfacial area transport equation gives a good prediction at the downstream from a certain distance regardless of the initial bubble size.

On the other hand, the one-group interfacial area transport equation suggests that for low liquid velocity, the initial bubble size may affect the interfacial area concentration even at the axial position far from the inlet. However, it is reported that the interfacial area concentration under steady fully developed bubbly flow conditions can be estimated by Eq. (30) with an average relative deviation of ±11.1%. Since the correlation was validated by 204 data sets taken by various investigators under extensive flow and loop conditions and does not have a term related to the initial bubble size, the slight difference in the initial bubble size may not affect the interfacial area concentration under steady fully developed bubbly flow conditions significantly except for some extreme flow conditions such as the introduction of slug bubbles in a stagnant liquid. This can be explained as follows. The difference in the initial bubble size between two different bubble number density conditions with the same flow condition is roughly in proportion to the −1/3 power of the ratio of the initial bubble number density, $n_{b,0}$. For example, the difference in the initial bubble size is estimated to be about 20% between $n_{b,0}$ and $0.5 \times n_{b,0}$, corresponding to $\Lambda_D = 0.8$ to 1.2. Thus, the bubble number density may not affect the initial bubble size so much. In addition to this, the strong bubble interaction much more than the present bubble coalescence and breakup models assuming an

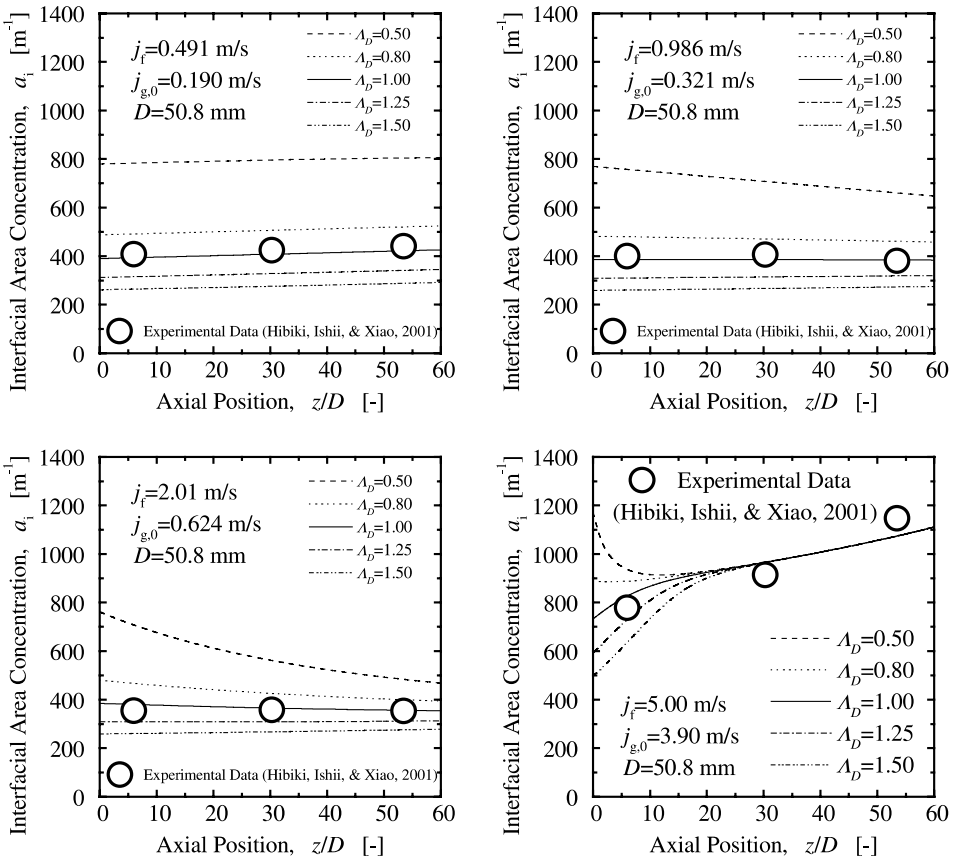

Fig. 13. Sensitivity analysis on initial bubble size.

isotropic turbulence can be expected in the vicinity of the inlet. The bubble size can increase or decrease near the inlet instantaneously to reach a range of a stable bubble size, which may be represented by Eq. (31). Thus, the present one-group interfacial area transport equation with the correlation of the initial interfacial area concentration would be promising for describing the interfacial area transport at the downstream of a certain distance from the inlet except for the vicinity of the inlet. For the application of the interfacial area transport equation to the flow very near the inlet, the interfacial area transport equation requires the modeling of the sink and source terms near the inlet by considering the effect of a bulk flow. The experimental work on this point should also be emphasized in a future.

3.8. Comparison of interfacial area concentration by interfacial area transport equation with that by TRAC-P code

In the present thermal-hydraulic system analysis codes, the effects of interfacial structure have been analyzed by using flow regimes and transition criteria. Determining the flow regime based on the values of the void fraction and mixture volumetric flux constitutes a static approach that does not dynamically represent the changes in the interfacial structure [2,3]. In the static approach, the flow regime is assumed to change instantaneously. In other words, no time or length scale is incorporated into the transition criteria. The interfacial structure is characterized by assigning an interfacial area concentration as a function of void fraction for each flow regime determined based on the value of the void fraction and mixture volumetric flux. Then, the magnitude of the interfacial transfer terms ($\sim a_i \times$ driving potential) is evaluated by utilizing the interfacial area concentration. Such the static approach causes a serious problem in calculating a developing flow. To exemplify how the current flow regime model could lead to instantaneous flow regime transition, Uhle et al. [3] applied RELAP5 code to the case of flow undergoing a transition from bubbly into horizontally stratified in a channel. Uhle et al. [3] also utilized TRAC-P and RELAP5 codes to model an axial development of the interfacial area concentration measured at Purdue University. It was shown that the approaches used by the system analysis codes were limited in their ability to model the true nature of flow regime development.

In what follows, it will be exemplified that the present thermal-hydraulic system analysis codes do not properly model the axial development of the interfacial area concentration. For example, in the TRAC-P code, the interfacial area concentration of bubbly flow is calculated by Eq. (22) with local void fraction and bubble diameter. In the TRAC-P code, the Sauter mean diameter is expressed as an approximate arithmetic mean between the minimum and maximum diameters observed experimentally, or equal to

$$D_b = 2Lo. \tag{38}$$

The comparison among experimental data by the present authors [26], TRAC-P calculation by Ishii et al. [11], and calculation by the one-group interfacial area transport equation developed in this study is performed here for the data sets taken in a 25.4 mm-diameter pipe under the flow conditions of $j_f = 0.872$ m/s and $j_{g,0} = 0.0813$ m/s ($\alpha_{z/D=125} = 0.0935$), and $j_f = 3.49$ m/s and $j_{g,0} = 0.702$ m/s ($\alpha_{z/D=125} = 0.195$). It should be noted here that the Sauter mean diameter calculated by Eq. (38) is 5.46 mm at 20 °C and atmospheric pressure. It can be seen from Eq. (22) that the interfacial area concentration calculated by the TRAC-P code is monotonically in proportion to the void fraction regardless of physical process governing the bubble coalescence and breakup. Fig. 14 depicts the axial developments of the interfacial area concentrations measured in the experiment as well as those predicted by the TRAC-P code and the interfacial area transport equation. Open and solid circles indicate the experimental data, and solid, broken and dotted lines indicate the interfacial area concentration changes predicted by the one-group interfacial area transport equation using the interfacial area concentration measured at $z/D = 12$ as the initial value, the one-group interfacial area transport equation using Eq. (31) to estimate the initial interfacial area concentration, and the TRAC-P code, respectively. It is apparent that the approach utilized by the TRAC-P code cannot predict accurate results for both flow conditions and proper trend for $j_f = 3.49$ m/s and $j_{g,0} = 0.702$ m/s.

For the flow condition of $j_f = 0.872$ m/s and $j_{g,0} = 0.0813$ m/s ($\alpha_{z/D=125} = 0.935$), the change of the interfacial area concentration predicted by the one-group interfacial area transport equation suggests that the bubble coalescence due to random collision between bubbles, and the bubble breakup due to random collision between bubble and turbulent eddy are not marked (see Fig. 15). Insignificant bubble coalescence may be due to insufficient bubble mixing length to cause the bubble random collision because of long distance between bubbles. Negligible bubble breakup may be attributed to the small turbulence fluctuation, where the turbulent eddies may not have enough energy to disintegrate the bubbles. These lead to a major role of the bubble expansion due to the pressure reduction along the axial direction. For this flow condition, the TRAC-P code gives the proper trend of the interfacial area concentration change along the flow direction but the large discrepancy in the interfacial area concentration is found due to improper determination of the Sauter mean diameter in the TRAC-P code. On the other hand, the one-group interfacial area transport equation can predict the proper trend as well as the accurate interfacial area concentrations.

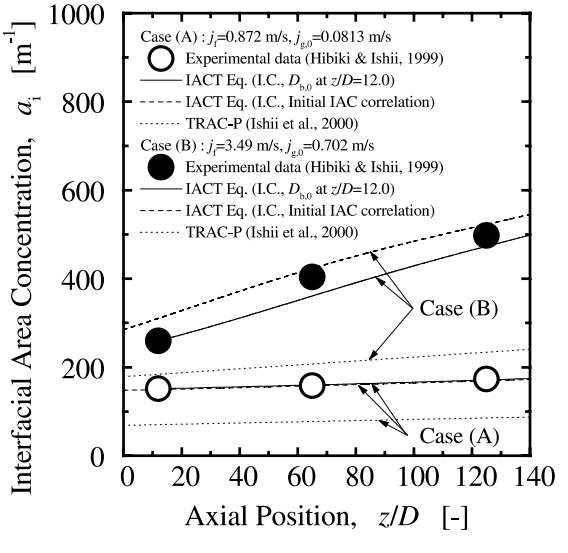

Fig. 14. Comparison between one-group interfacial area transport equation and TRAC-P code.

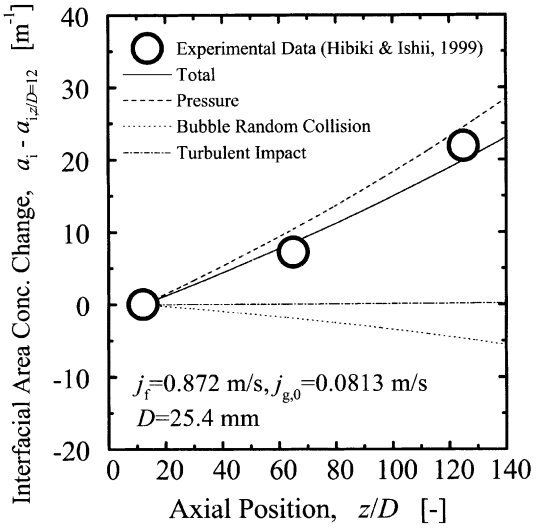

Fig. 15. Contributions of bubble coalescence, breakup, and expansion to interfacial area transport ($j_f = 0.872$ m/s, $j_{g,0} = 0.0813$ m/s).

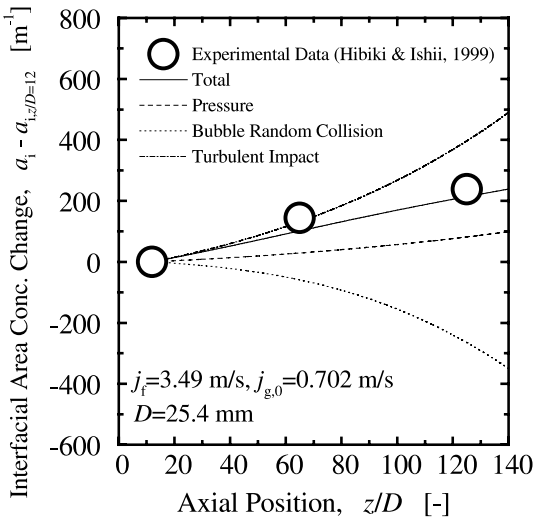

Fig. 16. Contributions of bubble coalescence, breakup, and expansion to interfacial area transport ($j_f = 3.49$ m/s, $j_{g,0} = 0.702$ m/s).

For a finely dispersed bubbly flow condition such as $j_f = 3.49$ m/s and $j_{g,0} = 0.702$ m/s ($\alpha_{z/D=125} = 0.195$), the strong turbulence disintegrates bubbles into small bubbles, resulting in marked increase of the interfacial area concentration (see Fig. 16). The strong turbulence increases the bubble breakup efficiency significantly. On the other hand, the large turbulence fluctuation may decrease the bubble contact time, resulting in the decrease of the bubble coalescence efficiency. Consequently, the bubble breakup rate becomes higher than the bubble coalescence rate. The increase of the interfacial area concentration in the flow direction is larger than that expected only by the bubble expansion. Because the TRAC-P code does not model the bubble coalescence and breakup processes, it failed to predict trends of the interfacial area concentration change. As shown in Fig. 14, the TRAC-P code fails to predict accurate value of the interfacial area concentration due to the improper determination of the Sauter mean diameter. On the other hand, the one-group interfacial area transport equation predicted both the proper trend and accurate value of the interfacial area concentration satisfactorily.

This study demonstrates that the derived one-group interfacial area transport equation would be promising for predicting the interfacial area transport of adiabatic air–water bubbly flows in medium pipes. However, to generalize the interfacial area transport equation, further analytical and experimental studies should be performed in other flow regimes, other fluid systems like steam–water flow system, and two-phase flows in various channels such as an elbow, a T-junction, and large and small channels. The introduction of two-group interfacial area transport equations should be indispensable in slug and churn flows. Additional bubble coalescence and breakup mechanisms such as wake entrainment, shearing-off, and surface instability should be considered to model the sink and source terms in the two-group interfacial area transport equations [7,10]. For the development of the interfacial area transport equation in boiling flows, additional sink and source terms due to phase change should be added in the interfacial area transport equation. The construction of rigorous data sets should be emphasized to obtain basic mechanisms to model the interfacial area transport phenomena and to evaluate the modeled sink and source terms. In view of this, experimental works have been initiated for slug and churn flow regimes [27], large diameter pipes [52], a small diameter pipe [53], subcooled boiling flow [28] and bubbly flow under microgravity environment [54]. These data sets will eventually be used for the development of general interfacial area transport equation.

4. Conclusions

To finalize one-dimensional one-group interfacial area transport equation in bubbly flow systems, this study has conducted the developments of (I) refined sink and source terms of the interfacial area concentration based on mechanisms of bubble–bubble and bubble–turbulent eddy random collisions, (II) the correlations of two adjustable variables in sink and source terms, and (III) the correlation of the initial interfacial area concentration. The finalized one-dimensional one-group interfacial area transport equation has been validated by 55 data sets taken in extensive adiabatic air–water bubbly flow conditions in four different vertical pipes (pipe diameter: 25.4–50.8 mm). The flow conditions of the data sets cover most of the bubbly flow regime, including finely dispersed bubbly flow and partly bubbly-to-slug transition flow (superficial gas velocity: 0.0144–4.88 m/s, superficial liquid velocity: 0.262–5.00 m/s, void fraction: 0.0124–0.443, interfacial area concentration: 22.1–1085 m^{-1}). Excellent agreement is obtained between predicted and measured interfacial area concentrations with an average relative deviation of $\pm 11.5\%$. Detailed discussions have been made on (i) the sensitivity analysis to the adjustable variables in the sink and source terms, (ii) the predominant term, (iii) the sensitivity analysis to the initial bubble size, and (iv) the comparison with TRAC-P code.

Acknowledgements

This work was performed under the auspices of the US Department of Energy's Office of Basic Energy Science. The authors would like to express their sincere appreciation for the encouragement, support and tech-

nical comments on this program from Drs. Manley, Goulard, and Price of DOE/BES. Part of this work was supported by grant-in-aid for Scientific Research from the Ministry of Education, Science, Sport and Culture (no. 12780385).

References

[1] D. Ebert (Ed.), in: Proceedings of OECD/CSNI Workshop on Transient Thermal-hydraulic and Neutronic Codes Requirements, NUREG/CP-0159, 1997.
[2] M. Ishii, Q. Wu, A. Assad, J. Uhle, Interfacial area transport equation for two-fluid model formulation, in: Proceedings of IMuST Meeting, 1998.
[3] J. Uhle, Q. Wu, M. Ishii, Dynamic flow regime modeling, in: Proceedings of the 6th International Conference on Nuclear Engineering, 10–14 May, 1998, San Diego, CA, USA, Paper no. ICONE-6509, 1998.
[4] M. Ishii, Thermo-Fluid Dynamic Theory of Two-Phase Flow, Eyrolles, Paris, 1975.
[5] M. Ishii, G. Kojasoy, Interfacial area transport equation and preliminary considerations for closure relations, PU/NE-93-6, School of Nuclear Engineering, Purdue University, USA, 1993.
[6] G. Kocamustafaogullari, M. Ishii, Foundation of the interfacial area transport equation and its closure relations, Int. J. Heat Mass Transfer 38 (1995) 481–493.
[7] Q. Wu, S. Kim, M. Ishii, S.G. Beus, One-group interfacial area transport in vertical bubbly flow, Int. J. Heat Mass Transfer 41 (1998) 1103–1112.
[8] Q. Wu, M. Ishii, J. Uhle, Framework of two-group model for interfacial area transport in vertical two-phase flows, Trans. ANS 79 (1998) 351–352.
[9] C. Morel, N. Goreaud, J.M. Delhaye, The local volumetric interfacial area transport equation: derivation and physical significance, Int. J. Multiphase Flow 25 (1999) 1099–1128.
[10] T. Hibiki, M. Ishii, Two-group interfacial area transport equations at bubbly-to-slug flow transition, Nucl. Eng. Des. 202 (2000) 39–76.
[11] M. Ishii, S. Kim, J. Uhle, Interfacial area transport: data and models, in: Proceedings of OECD/CSNI Workshop on Advanced Thermal-hydraulics and Neutronics Codes: Current and Future Applications, 10–13 April, 2000, Barcelona, Spain, 2000.
[12] A. Serizawa, I. Kataoka, I. Michiyoshi, Turbulence structure of air–water bubbly flow – I. Measuring techniques, Int. J. Multiphase Flow 2 (1975) 221–233.
[13] I. Kataoka, M. Ishii, A. Serizawa, Local formulation and measurements of interfacial area concentration in two-phase flow, Int. J. Multiphase Flow 12 (1986) 505–529.
[14] T.J. Liu, Experimental investigation of turbulence structure in two-phase bubbly flow, Ph.D. Thesis, Northwestern University, USA, 1989.
[15] I. Kataoka, A. Serizawa, Interfacial area concentration in bubbly flow, Nucl. Eng. Des. 120 (1990) 163–180.
[16] S. Kalkach-Navarro, The mathematical modeling of flow regime transition in bubbly two-phase flow, Ph.D. Thesis, Rensselaer Polytechnic Institute, USA, 1992.
[17] S.T. Revankar, M. Ishii, Local interfacial area measurement in bubbly flow, Int. J. Heat Mass Transfer 35 (1992) 913–925.
[18] S.T. Revankar, M. Ishii, Theory and measurement of local interfacial area using a four sensor probe in two-phase flow, Int. J. Heat Mass Transfer 36 (1993) 2997–3007.
[19] T. Hibiki, S. Hogsett, M. Ishii, Local measurement of interfacial area, interfacial velocity and liquid turbulence in two-phase flow, Nucl. Eng. Des. 184 (1998) 287–304.
[20] Q. Wu, M. Ishii, Sensitivity study on double-sensor conductivity probe for the measurement of interfacial area concentration in bubbly flow, Int. J. Multiphase Flow 25 (1999) 155–173.
[21] S. Kim, X.Y. Fu, X. Wang, M. Ishii, Development of the miniaturized four-sensor conductivity probe and the signal processing scheme, Int. J. Heat Mass Transfer 43 (2000) 4101–4118.
[22] W.H. Leung, S.T. Revankar, Y. Ishii, M. Ishii, Axial development of interfacial are and void concentration profiles measured by double-sensor probe method, Int. J. Heat Mass Transfer 38 (1995) 445–453.
[23] W.H. Leung, C.S. Eberle, Q. Wu, T. Ueno, M. Ishii, Quantitative characterizations of phasic structure developments by local measurement methods in two-phase flow, in: Proceedings of the 2nd International Conference on Multiphase Flow '95, Kyoto, Japan, IN2-17, vol. 1, 1995.
[24] C. Grossetete, Caracterisation experimetnale et simulations de l'evolution d'un ecoulement diphasique a bulles ascendant dans une conduite verticale, Ph.D. Thesis, Ecole Centrale Paris, France, 1995.
[25] S. Hogsett, M. Ishii, Local two-phase flow measurements using sensor techniques, Nucl. Eng. Des. 175 (1997) 15–24.
[26] T. Hibiki, M. Ishii, Experimental study on interfacial area transport in bubbly two-phase flows, Int. J. Heat Mass Transfer 42 (1999) 3019–3035.
[27] X.Y. Fu, Y. Mi, M. Ishii, Interfacial area measurement in a bubbly-slug transition air–water flow, in: Proceedings of the 8th International Conference on Nuclear Engineering, 2–6 April, 2000, Baltimore, USA, Paper no. ICONE-8327, 2000.
[28] Y. Mi, M. Ishii, R. Situ, M. Bartel, T. Masukawa, M. Mori, Local measurement of two-phase interfacial parameters in subcooled boiling, in: Proceedings of the 34th National Heat Transfer Conference, Pittsburgh, USA, 20–22 August, 2000, Paper no. NHTC2000-12000, 2000.
[29] T. Hibiki, M. Ishii, Z. Xiao, Axial interfacial area transport of vertical bubbly flows, Int. J. Heat Mass Transfer 44 (2001) 1869–1888.
[30] T. Hibiki, M. Ishii, One-group interfacial area transport of bubbly flows in vertical round tubes, Int. J. Heat Mass Transfer 43 (2000) 2711–2726.
[31] H. Städtke, A. Blahak, B. Worth, Modelling of transport of interfacial area concentration in two-phase flow systems, in: Proceedings of the 8th International Topical Meeting on Nuclear Reactor Thermal-Hydraulics, Kyoto, Japan, vol. 1, 1997, pp. 69–78.
[32] M.J. Prince, H.W. Blanch, Bubble coalescence and break-up in air-sparged bubble columns, AIChE J. 36 (1990) 1485–1497.
[33] M. Millies, D.A. Drew, R.T. Lahey Jr., A first order relaxation model for the prediction of the local interfacial

area density in two-phase flows, Int. J. Multiphase Flow 22 (1996) 1073–1104.
[34] L.B. Loeb, The Kinetic Theory of Gases, Dover, New York, 1927.
[35] T. Inui, A. Nakahara, O. Yamauchi, Y. Yoshikawa, Chemistry, Kagaku Dojin, Kyoto, Japan, 1975.
[36] C.A. Coulaloglou, L.L. Tavlarides, Description of interaction processes in agitated liquid–liquid dispersions, Chem. Eng. Sci. 32 (1977) 1289–1297.
[37] T. Oolman, H.W. Blanch, Bubble coalescence in air-sparged bioreactors, Biotechnol. Bioeng. 28 (1986) 578–584.
[38] T. Oolman, H.W. Blanch, Bubble coalescence stagnant liquids, Chem. Eng. Commun. 43 (1986) 237–261.
[39] V.G. Levich, Physicochemical Hydrodynamics, Prentice-Hall, Englewood Cliffs, NJ, USA, 1962.
[40] R.D. Kirkpatrick, M.J. Lockett, The influence of approach velocity on bubble coalescence, Chem. Eng. Sci. 29 (1974) 2363–2373.
[41] W.K. Kim, K.L. Lee, Coalescence behavior of two bubbles in stagnant liquids, J. Chem. Eng., Jpn. 20 (1987) 449–453.
[42] C. Tsouris, L.L. Tavlarides, Breakage and coalescence models for drops in turbulent dispersions, AIChE J. 40 (1994) 395–406.
[43] D. Azbel, Two-phase Flows in Chemical Engineering, Cambridge University Press, Cambridge, MA, UK, 1981.
[44] D. Azbel, I.L. Athanasios, A mechanism of liquid entrainment, in: N. Cheremisinoff (Ed.), Handbook of Fluids in Motion, Ann Arbor Science, Ann Arbor, MI, 1983.
[45] J.O. Hinze, Turbulence, McGraw-Hill, New York, 1959.
[46] J.C. Rotta, Turbulence Stromungen, B.G. Teubner, Stuttgart, Germany, 1972.
[47] G. Kocamustafaogullari, W.D. Huang, J. Razi, Measurement of modeling of average void fraction bubble size and interfacial area, Nucl. Eng. Des. 148 (1994) 437–453.
[48] R.W. Lockhart, R.C. Martinelli, Proposed correlation of data for isothermal two-phase, two-component flow in pipes, Chem. Eng. Progr. 5 (1949) 39–48.
[49] T. Hibiki, M. Ishii, Interfacial area concentration in steady fully-developed bubbly flow, Int. J. Heat Mass Transfer (2001) 3443–3461.
[50] M. Millies, D. Mewes, Interfacial area density in bubbly flow, Chem. Eng. Process. 38 (1999) 307–319.
[51] Y. Taitel, D. Bornea, A.E. Dukler, Modelling flow pattern transitions for steady upward gas–liquid flow in vertical tubes, AIChE J. 26 (1980) 345–354.
[52] T. Smith, M. Ishii, X. Sun, S. Kim, J. Uhle, Interfacial area transport in large diameter pipe (4″ and 6″), in: Proceedings of the 4th International Conference on Multiphase Flow, 27 May – 1 June, 2001, New Orleans, USA.
[53] T. Hibiki, T. Takamasa, M. Ishii, Interfacial area transport of bubbly flow in a small diameter pipe, J. Nucl. Sci. Technol. 38 (2001) 614–620.
[54] T. Takamasa, T. Iguchi, T. Hazuku, T. Hibiki, M. Ishii, Interfacial area transport of bubbly flow under microgravity environment, in: Proceedings of the 4th International Conference on Multiphase Flow, 27 May – 1 June, New Orleans, USA, 2001.